FACULTY OF SCIENCE
UNIVERSITY OF COPENHAGEN

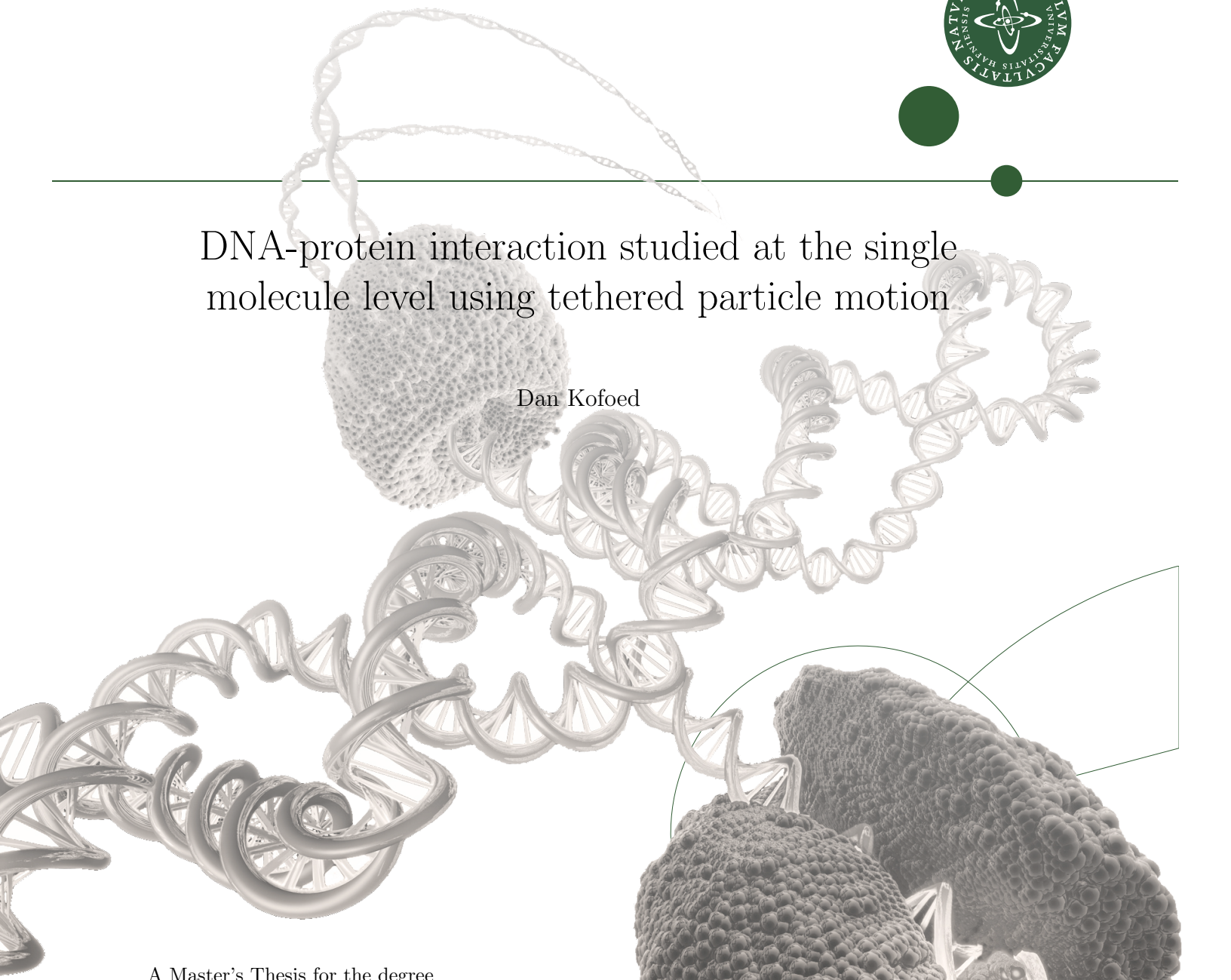

DNA-protein interaction studied at the single molecule level using tethered particle motion

Dan Kofoed

A Master's Thesis for the degree
Cand. Scient Nanoscience
Niels Bohr Institute
University of Copenhagen
August 2, 2012

Supervisor: Lene B. Oddershede
Co-supervisor: Michael Lisby

Abstract

This thesis report consists of two projects based on tethered particle motion (TPM) in which a polystyrene sphere (a bead) of half a micron in diameter is tethered by a DNA molecule to a surface and thereby used as a probe which can be observed and manipulated. This setup is named a bioassay. The first project is about the enzyme topoisomerase IA which relaxes negatively supercoiled DNA. Together with the enzyme gyrase, which introduces negative supercoils in DNA, topoisomerase IA regulates the degree of supercoiling in prokaryotes. Topoisomerases are present through all three domains of life and are highly conserved which indicate their vital role in fundamental cellular processes like replication and transcription.

In the present study topoisomerase IA activity was tested with a native distribution of supercoiled plasmids from *E. coli*. Restricted Brownian motion of a bead was visualized from the amplitude of fluctuations in a focal plane. Only in one occasion changes in average bead motion were found. The change in motion was reversibil which is not in accordance with topoisomerase IA's enzymatic pathway. Steric hinderence associated with the bioassay could explain the reversible obersvation but is highly hypothetical as lack of reproducibility prevents any conclusions on characteristic behavior to be drawn.

The second project was on the protein Rdh54's role in resolving anaphase bridges which are concatenated DNA threads occuring during mitosis. The anaphase bridges span sister chromatids and their resolution are vital for successful chromosome segregation. Through mechanistic interaction it is possible that Rdh54 located on DNA can open a spatio-temporal window which allows the anaphase bridges to be resolved by topoisomerase II while sister chromatids move apart. Other studies have suggested that this is the role of the proteins PICH and BLM [19]. A key protein complex counteracting this spatio-temporal window is the histone complex which wraps DNA around itself (then named nucleosome).

As in project one a TMP bioassay was established to be able to visualize Rdh54 located and translocating on DNA. Furthermore a R-loop construct was planed to be included in the bioassay. The R-loop would serve as a probe to test whether Rdh54 could remove obstacles on DNA when translocating. This would be interesting to test in relation to Rdh54's role of opening a spatio-temporal window because one way to prevent nucleosomes from occuring in DNA is to mechanically remove them. A lot of time was spend on establish the bioassay and the project is far from done and in its present form it constitutes a research proposal which is presented here.

Resumé

Denne specialereport består af to projekter baseret på metoden "tethered particle motion" (TPM), som benytter en polystyren sfære (en bead) med en diameter på en halv mikrometer fastgjort til en overflade vha. et DNA molekyle, som derved fungerer som en probe, der kan observeres og manipuleres. Dette setup kaldes et bioassay. Det første projekt omhandler enzymet topoisomerase IA, som løser negativt supercoilet DNA. Sammen med enzymet gyrase, som introduserer negative supercoils i DNA, regulerer topoisomerase IA graden af supercoiling i prokaryoter. Topoisomeraser er at finde i alle biologiens tre domæner og er vel bevarede gennem evolutionen, hvilket indikerer deres livsnødvendige rolle i fundamentale celluære processer som replikation og transkription.
I dette studie af topoisomerase IA blev dets aktivitet testet med en naturligt forekommende distribution af supercoilede plasmider fra *E. coli*. Begrænsede brownske bevægelser foretaget af et bead blev visualiseret via amplituden af fluktuationerne i et fokuseringsplan. Kun i et tilfælde kunne en ændring i den gennemsnitlige bevægelse af beaden observeres, men bevægelsen var reversibel, hvilket ikke er i overensstemmelse med topoisomerases enzymatiske reaktionsvej. Sterisk hindring i bioassayet kan forklare den reversible bevægelse men er højst hypotetisk i og med, at manglen på reproduserbare resultater forhindrer en sikker karakteristik af reversibel opførsel.
Det andet projekt omhandlede proteinet Rdh54 og dets rolle i udredningen af anafasebroer, der er sammenkædede DNA tråde, som optræder under mitosen. Anafasebroerne er udspændt mellem søsterkromatider, og deres udredning er essentiel for, at kromosomer kan segregere fuldstændigt. Gennem mekanisk interaktion kan Rdh54 lokaliseret p DNA muligvis skabe et tidsrum, som tillader udredingen at anafasebroerne vha. topoisomerase II samtidig med at søsterkromatiderne bevæger sig fra hinanden, hvilket et andet studie har foreslået er proteinerne PICHs og BLMs rolle [19]. Et proteinkompleks, som har en hovedrolle i at modarbejde dette tidsrum er histonekomplekset, som pakker DNA rundt om sig (og dermed bliver et nukleosom).
Ligesom i det første projekt blev et TPM bioassay udviklet for at viualisere Rdh54s lokalisering og bevægelse på DNA. Derudover blev det planlagt at inkludere et R-loop i bioassayet, som skulle bruges til at teste Rdh54s evne til at skubbe forhindringer af DNA når Rdh54 bevæger sig. Dette ville være interessant at undersøge i forhold til Rdh54s rolle i at skabe et tidsrum, fordi en måde at forhindre nukleosomer i at optræi DNA er ved mekanisk at fjerne dem. Meget tid gik med at danne bioassayet, og derfor er projektet langt fra færdigt, og i sin nuværende form udgør det et forslag til, hvordan et studie af Rdh54 kan foretages. Dette forslag presenteres her.

Dan Kofoed, 160983–1169

Date

Acknowledgements

A word of thanks goes to all the people in my Optical Tweezers Group at Niels Bohr Institute, Copenhagen. To my supervisor and head of the group Lene B. Oddershede for her great patience and encouraging words in times of unsuccesful experiments which by far exceeded times of successful ones. To Kamilla for introducing me to the laboratory work and pass on the experimental tips and tricks that makes all the difference, for her demonstration of the tethered particle motion technique, and for her kind invitation to proofread the thesis. To Rebecca for getting me started on the NanoTracker setup (to bad the experiments did not turned out to be fruitful). To Anders and Pradeep for giving a helping hand on conducting fluorescence experiments. To Stanley Brown for his help with gel electrophoresis and his indispensable expertise and contribution to putting the bioassay together. To Michael Lisby who was my cosupervisor and his fellow workers at Biocenter, Institute of Biology, Copenhagen, for their cooperation in the Rdh54 project. Last but not least a special thanks goes to whoever responsible for keeping the espresso machine up and running and to whoever kept the tempting summer weather on hold while I was writing the thesis report.

Contents

Chapter 1

Introduction

This master thesis consist of two projects. The first is on the subject of the enzyme topoisomerase IA from *E. coli* and its ability to relax torsional strain in DNA known as supercoils. The second is on the protein Rad homolog 54 (Rdh54) and its role in the mechanism of resolving anaphase bridges: concatenated DNA strands hindering the ongoing process of chromosome segregation during mitosis.

Relaxation of supercoils in DNA has been studied on a single molecule level before [21, 16]. In those studies a constraint linear DNA molecule was twisted to make it form supercoils. The method was therefore invasive in its introduction of supercoils. The aim of this thesis was to study the removal of already present native supercoils from single circular *E. coli* DNA molecules named plasmids. A plasmid was tethering a single particle to a surface and brownian motion of the particle was observed through video microscopy. The obstacle of preserving the plasmid in a closed circular native state while using it as a tether was solved with the use of peptide nucleic acids handles. This had been done in earlier studies perfomed in my Optical Tweezers Group and the project on topoisomerase was partly an adaptation of such a study by Kamilla Nørregaard, Niels Bohr Institute, KU, from her master thesis. I used the same experimental setup and video microscopy analysis to study topoisomerase as she used to study protein mediated DNA looping [32].

The aim of the second project was to establish a procedure for studying the binding and translocation of Rdh54 along DNA on a single molecule level. Rdh54 has been found present at DNA between sister chromatids during segregation. In mutants lacking the protein the segregation fails. It is speculated that Rdh54 is involved in keeping DNA free of nucleosomes in early stages of segregation to allow sister chromatids to separate while they are still linked by DNA called anaphase bridges [19]. This provides a spatio-temporal window in which the cell has time to resolve the anaphase bridges and complete the segregation successfully. The mechanism is not fully understood. To get insight in Rdh54's function it would be interesting to study its ability of clearing obstacles along DNA and its behavior in a system under tension. Single molecule techniques are well suited for such studies

and especially the optical tweezers technique has proven excellent in studying mechanistic behavior of proteins as it can measure and apply forces on the molecular level in the pico newton regime. One goal of the project was therefore to establish a bioassay with DNA tethered particles which can be manipulated through the use of an optical tweezer and to study the behavior of Rdh54 through fluorescence microscopy. The project on Rdh54 was in collaboration with Michael Lisby and his group at Department of Biology, Copenhagen Biocenter, KU. They study the role of Rdh54 and the mechanisms by which it works and Michael provided the protein and DNA construct used in the bioassay for the present thesis. Because of experimental difficulties and time limits it was only possible to carry out studies on Rdh54 in a proof-of-concept manner. This means that the development of the experimental method and the data acquisition have not been completed but the fundamental concepts of how to carry out the experiments have been tested. The project will therefore be presented as a research proposal.

Similar bioassays in both projects.

The experimental sample used in both projects is similar in design and preparation. It is a bioassay in which a single DNA molecule tethers a single microsphere also called a bead. The double stranded DNA molecule, being only approximately 3 nm wide, is not visible in a microscope. When the bead, which is ~ 0.5 μm in diameter, is attached to the DNA, it works as a visible probe. In the topoisomerase project the bead motion was used to probe the conformational state of a supercoiled *E. coli* plasmid. The enzymatic action of topoisomerase on relaxing supercoiled DNA can hence be observed through an increased amplitude of bead motion. Observations were made through video microscopy from which the bead motion was analyzed. In the Rhd54 project the bead was used to first localize a 16 μm long DNA molecule and next to manipulate the DNA using an optical trap. The bead can be trapped by a laser and thus the DNA can be stretched and positioned in a controlled manner. Rdh54 proteins had fluorophores bound to them and they were observed through confocal fluorescence microscopy.

Why two projects?

The second project on Rdh54 was originally thought to be the only project of this thesis. An essential part of the experimental setup was to tether a bead to a surface through DNA. To establish a decent amount of well defined tethered beads on a regular basis turned out to be difficult and so the very fundament of the bioassay did not function properly in the first half of the thesis. The laboratory work in this phase was spend on adjusting the DNA construct preparation and the buffers in which the tethers were assembled. The unsuccessful tests compelled a back-up plan which led to the project on topoisomerase. The experimental setup in this project had already been developed and proven functional and reliable. The bioassay also consisted of a tethered bead but the DNA construct was different

in that it was a circular supercoiled DNA of much smaller size. It was therefore not suitable for studying Rdh54 on DNA as the bead would cover the fluorescence signal from Rhd54 and the plasmid would be to small and supercoiled to properly study the translocation of the protein along the DNA. Instead it was decided to study the topoisomerase on this construct.
The two projects will be presented separately as part I: "Supercoil relaxation by topoisomerase IA" and as part II: "Rdh54 behavior on DNA".

1.1 Single molecule experiments

Experiments on the single molecule level stands in contrast to bulk experiments where millions of molecule interactions can be studied at once. Bulk experiments can reveal molecular properties in a homogenous perspective as the results are an average of molecule interactions. Furthermore, bulk experiments allow studies of molecules in a crowded environment similar to the native environment inside a cell. In contrast, single molecule experiments can reveal distributions of molecular properties hidden in the average and study the possible subpopulations of interactions. Furthermore, the single molecule techniques can be used to mechanically manipulate individual molecules and to study enzymes in real time. The two types of experiments hence complement each other as they give a distribution of properties on different scales. The drawbacks of the time consuming single molecule experiments are the small statistical basis and the interference with the system using probes like beads or fluorophores attached to molecules. Furthermore, the measurements are often influenced by noise to a great extend. At the microscopic level the thermal motion, causing e.g. particles to make Brownian motion, is dominant.
Typical single molecule techniques counts optical and magnetic tweezers, or atomic force microscopy (AFM), and often in combination with single molecule fluorescence techniques like Total Internal Reflection Fluoresence (TIRF) or Förster Resonance Energy Transfer (FRET). E.g., interactions of molecular motor proteins like RNA polymerase, important in transcription, have been investigated with these techniques [6]. Enzymatic step sizes, rates constants for dissociation and processivity (e.g the number of nucleotides added per dissociation step of a polymerase) are measured during such experiments. Also properties of a DNA molecule itself has been studied through force-extension measurements made possible with optical and magnetic tweezers. By twisting and stretching the molecule a model for elasticity has been made: the worm-like chain model, or if helical structure and sequence are taken into account as well: the twistable worm-like chain model [18]. These properties are important as DNA are kept under tension by proteins inside the cell and hence DNA-protein interactions are inflicted by the topological state of DNA. An especially important enzyme in relation to DNA tension, and subject of one of the projects described in this report, is topoisomerase. The mechanism of topoisomerase IA and IB has

been investigated with the use of magnetic tweezers [16, 21]. A magnetic bead controlled via a magnetic field was used to induce supercoils in a DNA molecule which results in a decreasing DNA end-to-end distance. After addition of enzyme they used the bead as a probe to observe supecoil relaxation by the change of the end-to-end distance. In this way they found the distribution of supercoil relaxation step sizes. The experiments suggested how to model the mechanics behind enzymatic cycles of topoisomerases. (More on the models in section 2.2).
Other single molecule studies of DNA-protein interaction has demonstrated the ability of the technique to refine the knowledge of reaction pathways. One such study on the TATA-box binding protein was made with the combination of tethered particle motion and video microscopy [41]. Through the Brownian motion of a bead attached to a DNA molecule the authors observed the stepwise binding of the protein to DNA and identified an additional state of the reaction pathway not known or predicted from previous ensemble studies. The same technique is used in the topoisomerase study presented in this thesis.
The single molecule conditions for DNA and bead interactions, described in this report, were controlled by scaling down the concentrations of reagents, to a level where the probability that only one DNA molecule binds one bead was largest and still happened on a reasonable time scale. By so creating single molecule conditions the powerful techniques of video microscopy, tethered particle motion, fluorescence and optical tweezers were applied in the present study to investigate DNA-protein interaction.

Part I

Supercoil Relaxation by Topoisomerase IA

Chapter 2

Supercoils and Topoisomerases

Ever since James D. Watson and Francis Crick, with the help from Rosalind Franklin's x-ray diffraction image, solved the molecular structure of DNA and showed that it was a double helix, models have been proposed, on how this biopolymer regulates the transfer of information from our genes: the transcription and replication. The regulation involves unwinding and overwinding of the DNA double helix which alters its structural form. Overwinding causes the helix to form structures called supercoils because of fundamental mechanical properties attributed to polymers. Such topological states of DNA can be changed by a group of enzymes called topoisomerases. The interplay between topological torsion in DNA, especially supercoils, and topoisomerase is therefore of fundamental importance to understand the expression and regulation of genes.

2.1 Supercoiling and linking number

The molecular structure of DNA implies a natural winding of two strands around an axis called the helical axis. This stabilized structure is referred to as the DNA double helix and a model of it can be seen in figure 2.1a. DNA supercoiling denotes the over- or underwinding of the DNA double helix. Imagine holding a rubber band stretched between your fingers.[1] If you begin to twist the ends, strain is build up in the band. If you move the two ends closer together the band will wind around itself to balance out the twisting strain. A DNA double helix shows the same behavior as the rubber band and the intertwined helix structure is named plectonemic supercoils [25]. The plectonemic supercoils can be seen in figure 2.1b. In a closed loop of a double helix, like that of a plasmid, there exist a balance between helical twists and supercoils given by the linking number Lk:

[1] Find a rubber band included in the back of the report.

$$Lk = Tw + Wr, \tag{2.1}$$

where Tw is the number of turns around the helical axis also called twists, Wr is the number of supercoils also called writhes, and Lk is the number of times each strand twist around each other. The topology of DNA can therefore be quantified in terms of Lk, Tw and Wr. To visualize the relation between Tw and Wr for a plasmid, a ribbon can be used [25].[2] Hold the ribbon by its ends and bring the two ends together to form a loop. Before you close the loop make one full rotation of one end of the ribbon, which is to say $\Delta Tw = 1$. When closing the loop you see one plectonemic supercoil (one writhe) forming. This illustrates the convention: *one supercoil is introduced into a DNA loop by one full turn of one end around the helical axis of a double helix* [46]. The supercoil is positive if the twist overwinds a right-handed helix and negative if it underwinds the helix.

Figure 2.1: (a) A model of the DNA double helix. The two ribbons symbolize the sugar-phosphate backbones and the rods pairs of bases. The helical axis is indicated by the vertical line. [48]. (b) Plectonemic supercoils in plasmids with negative and positive writhes. [45].

The change in linking number, ΔLk, from the relaxed state, Lk_0, can only happen to a certain degree before the double helix becomes unstable. If the helix is underwind to an extreme, base paring will be interrupted and the DNA will melt. The range in which the double helix is stable can be expressed by the limits of the fraction $\frac{\Delta Lk}{Lk_0}$ which is approximately [-0.1 ; 0.1] for a closed DNA loop [25]. A relaxed DNA double helix has 10.5 bp per turn on average. For a plasmid of 7600 bp (the size used in this experimental work) this gives roughly $Tw = 724$ which equals Lk_0 in the relaxed state where $Wr = 0$. Using the limits [-0.1 ; 0.1] ΔLk can be found: $\Delta Lk = \pm 0.1 \cdot Tw \approx \pm 72$.

[2] A paper ribbon is included in the back of the report.

2.2 Topoisomerase I and II

Topoisomerase are enzymes that regulate DNA topology by changing the linking number, Lk. They are divided in type I and II depending on whether they cut a single strand or both strands of a DNA double helix. A single strand is made of a backbone (a sugarphosphate polymer) with its bases and two combined strands comprise a DNA double helix. Topoisomerases can be further subdivided in subfamilies which differ in structure and mechanics but have the binding to DNA in common. Topoisomerase covalently bind through a phosphordiester linkage from a tyrosine residue to a phosphate group in the backbone of a DNA strand. This transesterfication creates a nick in the strand which can be rejoined by the reverse reaction [46]. The nicking of a single strand leads to supercoil relaxation through two distinct mechanisms related to the type I enzymes.

Enzyme-bridging mechanism.

This mechanism operates with a strand-passage event in which one single strand of a DNA double helix is passed through the other. The mechanism is associated with topoisomerase IA and consistent with its crystal structure illustrated in figure 2.2a [11]. In order for one strand to pass the other they the bases must be unpaired in that local region. An underwind DNA double helix has less stabilized base paring and is closer to a single strand state than relaxed or overwound DNA is. Topoisomerase IA primarily binds and processes negatively supercoiled DNA because it more easily can unpair bases of destabilized strands. (It has been shown that it can process positive supercoils too, but it requires a DNA region in which the strands are unpaired [11]). After binding, one strand is nicked through transesterfication and the enzyme binds now both nicked ends bridging the strands. In this open state the second strand can pass trough the first and into the enzyme cavity. The enzyme goes to the closed state when the nick is resealed and an enzyme-bridging strand passage has occurred. The final step is again an opening event in which the enzyme releases the passed strand. One enzymatic cycle is therefore given as: cleavage and opening of strand $\rightarrow$ strand passage $\rightarrow$ closing and religation $\rightarrow$ opening and release. This indicates that only one supercoil can be relaxed per cycle, $\Delta Lk = 1$, as have been confirmed by V. Croquette and co workers from single molecule experiments using a magnetic tweezer [16]. The relaxation by topoisomerase IA happens without an energy source like ATP. Instead the energy that drives the reaction comes from the stored tension in DNA. Mg^{2+} must be present as it is required at a specific enzyme domain in order for conformational changes to occur. The direction of the strand passing process comes from the negatively supercoiled DNA [10].
Because topoisomerase IA relaxes negative supercoils it is believed to balance the degree of negative supercoiling induced by the topoisomerase enzyme gyrase (a type II A) in *E. coli* [11]. The genome must maintain a level of negative supercoils to remain compact and induce processes that requires local unwinding of the double helix. Therefore it is crucial

to control this balance for the organism.

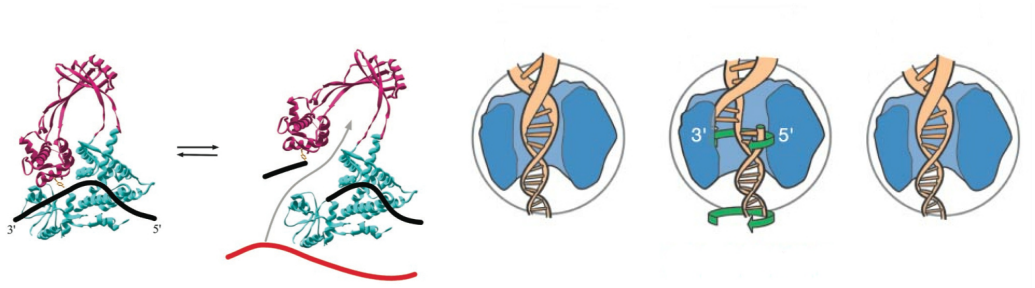

(a) (b)

Figure 2.2: The two mechanisms of supercoil relaxation done by topoisomerase type I . (a) The enzyme-bridging strand passage mechanism of *E. coli* topoisomerase IA [11]. Going from the closed to the open form the enzyme creates a nick in the single stranded DNA (black) where another strand (red) can pass through. (b) The swirling mechanism of topoisomerase IB [21]. After a nick is created in the DNA the upper part of the strand is held tight in the enzyme cavity while the lower part rotates releasing the strain stored in the DNA.

Strand-rotation mechanism.

The other mechanism associated with type I topoisomerase involves a swirling motion as illustrated in figure 2.2b [21]. This mechanism is associated with topoisomerase IB. When the enzyme binds the DNA double helix it creates a nick in one strand through transesterfication. The 5' end of the broken strand is not bound by the enzyme and can rotate around the intact strand releasing tension in the helix. In this way topoisomerase can relax both positively and negatively supercoiled DNA by allowing bidirectional change in twists. The enzyme forms a clamp around the double helix in which a friction occurs with the rotating strand. Hence the enzyme does not release all supercoils at once down to a relaxed state but instead in steps (ΔLk) of varying sizes. The larger torque stored in DNA, the larger steps the enzyme relaxes. The friction increases the probability of religation of the nicked strand while the torque stored in the helix decreases it [21]. The swirling mechanism hence allows the enzyme working rate to be controlled by the supercoiled state of DNA – it only relaxes DNA to the extend that is needed.
All organisms have at least one type of topoisomerase IA. Topoisomerase IB is widely present in the three branches of life; eukarya, archaea, and bacteria but not in the particular organism *E. coli*. All organisms also have at least one type II topoisomerase.

Topoisomerase II

Topoisomerase II facilitates the passage of a complete double helix strand through another and alters thereby ΔLk by two. The process is carried out with the energy consumption of ATP. The mechanism of topoisomerase IIA, like that of the bacterial gyrase, is shown in figure 2.3. The enzyme has a binding site for the DNA strand about to be transferred, T, in the top cavity. When T is in place the gating strand, G, is cleaved and the gate opens which allows the T strand to be transported through to the lower cavity. The G strand is religated and the T strand is released and finally the top cavity is reopened. The strand passage combines the binding and release of ATP with DNA interactions in a not fully understood coordination of a series of conformational changes [10, 22]. The overall mechanism is known though. After the G strand is bound, ATP binding causes closing of the top gate. If the T strand is present in the gate, the G strand is cleaved and the gate opens. The lower cavity opens by hydrolysis of an ATP to ADP and the T strand is released. The final reopening of the top cavity happens when ADP and P are released and one enzymatic cycle is complete.

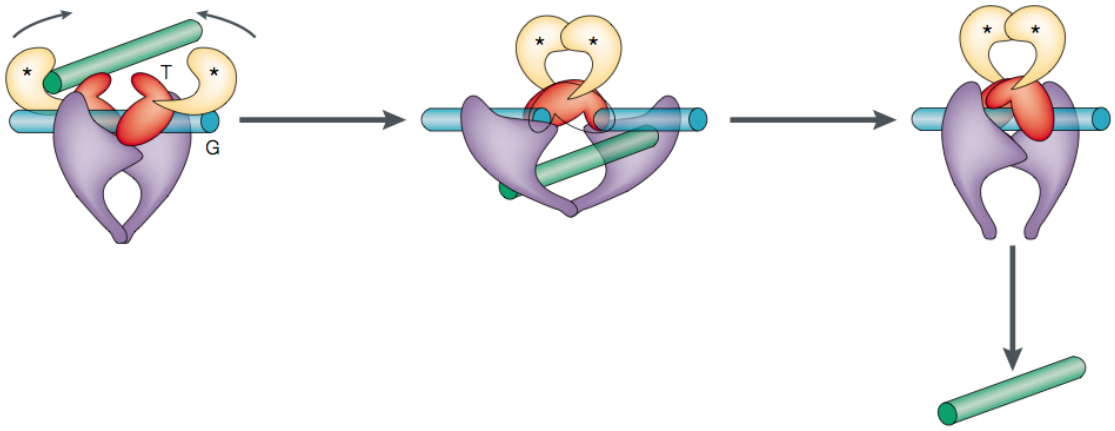

Figure 2.3: The mechanism of topoisomerases IIA (like that of gyrase) [46]. The $*$ represents ATP binding sites. The transferred DNA strand, T, is captured in the top cavity and the gating DNA strand, G, is cleaved. The gate opens and the T strand is transported through to the lower cavity. After religation of the G strand, the T strand is released and finally the top cavity reopens. The mechanism can relax supercoiled DNA as well as introduce negative supercoils in the case of gyrase.

How the two strands are orientated before the passage decides whether supercoils are relaxed or introduced into the DNA. In the case of gyrase the mechanism introduces negative supercoils (which can cancel positive supercoils) in the double helix. Gyrase has a domain

that wraps the DNA in a way that causes the two strands to be twisted around each other after strand passage. This leads to the introduction of negative supercoils.

2.3 Fundamental gene expression

The storage and transfer of information are universal throughout most organisms and are therefore called *the central dogma of molecular biology*. It states that information flows from DNA to DNA (replication) and from DNA to RNA (transcription) and from RNA to protein (translation). There are special cases that take other information flow routes but it has never been observed that information flows from proteins to other proteins, RNA, or DNA.
Two steps of the central dogma are related to this project. 1) The replication step necessary to duplicate the genome before mitosis (cell division), in DNA repair (through homologous recombination), and in genetic recombination. 2) The transcription necessary to make RNA copies that either folds into enzymes themselves or pass on information to produce proteins, and in DNA repair (through replicative repair). Both of these steps involve topoisomerase.

Replication

The DNA double helix is stabilized by the hydrogen bonds formed between base pairs on each strand. In order for enzymes to replicate the double helix strand, it must locally unwind to expose the bases that are about to be copied. DNA polymerase is the central enzyme that replicates DNA. Together with other enzymes and proteins it forms the replisome, which is a large complex that processes through the double helix strand while synthesizing new strands. In the replisome the helicase enzyme unwinds the double helix like a zipper but encounters a winding problem in the process. Imagine two intertwined threads representing the double helix, and a pencil interlaced in the thread, representing the replisome. If the pencil is forced through the windings towards one end without rotating itself, the intertwined threads begins to rotate. If the ends are restricted from rotating, tension builds up and the threads tangle up to compensate the tension in the overwind state because this is energetically more favorable. The same happens in front of the replisome as illustrated in figure 2.4.
The rotational drag restricts it from rotating around the helical axis. Instead the double helix overwinds because the DNA strand is to long to be freely rotating as well. In prokaryotes the DNA double helix is a circular plasmid and therefore naturally restricted, it cannot make a compensating free rotation in response to unwinding. In addition if the replisome also can not rotate around the helix, positive supercoils forms in front of it as a result. The cell must deal with the supercoils to prevent the replisome from stalling for

which it uses topoisomerases.
The swivel mechanism related to the activity of topoisomerase IB constantly relaxes short lengths of the helix in front of the replisome while the complex moves forward. When the genome has been replicated it would be entangled to an extend that would prevent segregation during mitosis if it was not for the action of topoisomerase type II. The mechanism of passing double helices through each other untangles the duplicated genomes which consequently can be separated successfully into two daughter cells.

Transcription

As in replication, the DNA double helix needs to locally unwind in transcription. One strand is used as template and a complementary messenger RNA strand (mRNA) is synthesized. In transcription the RNA polymerase complex induces tension as it processes through the double helix. The complex is connected to the synthesized mRNA which again is connected with ribosomes that translate it in the case of prokaryotes or with the spliceosome in case of eukaryotes. This means that the complex is not free to rotate while the DNA unwinds. Instead DNA is twisted and forms positive supercoils in front and negative supercoils behind the transcription site, known as the twin-supercoiled domain illustrated in figure 2.5 [46].
Supercoils are actually already present in DNA before replication and transcription takes place and they facilitate the initiation of these processes. When the right-handed double helix unwinds (is opened), it induces positive supercoils as a response to overwinding. Negative supercoils on the other hand are formed as a response to underwinding and reduces the helical tension. Negative supercoils can therefore initiate an opening of the double helix. *E. coli* uses a type of topoisomerase called gyrase to introduce such negative supercoils in DNA to maintain helical tension. Positive supercoils arising from the opening of the helix cancel out nearby negative supercoils. The helical tension is then restored with the use of gyrase [1].

DNA packaging.

DNA packaging is necessary for the cell to maintain the genome in a controlled state. The genome has to be compact to fit inside a cell. The human genome of 46 chromosomes is 2 meters long but must fit inside the nucleus of 6 μm [1] and the genome of *E. coli*, measuring 1.4 mm, is 1000 times longer than the organism itself [42]. The compact DNA molecule should still be accessible to enzymes and proteins for replication, repair and transcription to be carried out. This requires a high level of organization. In eucaryotes DNA is packed into chromatin fibers consisting of complexes of proteins that fold supercoiled DNA into compact structures called nucleosomes. In prokaryotes the genome consist of one large circular DNA but is not organized with chromatin structures. Instead the DNA is compacted through plectonemic supercoils as a consequence of its circular constraint nature.

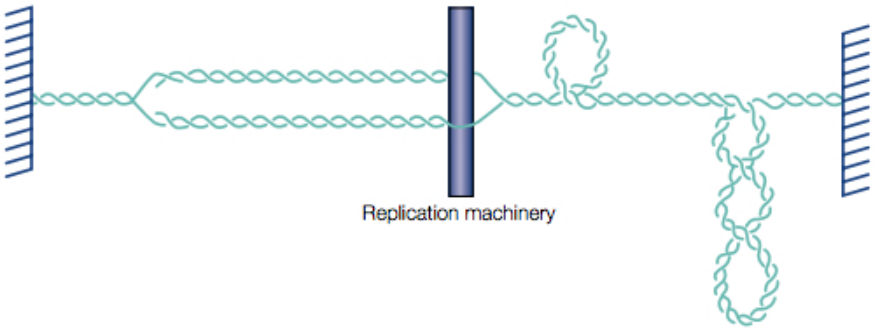

Figure 2.4: The Replication machinery processing through the DNA double helix. Positive supercoils are accumulated in front of the replication machinery when the DNA double helix is restricted from rotating.[46].

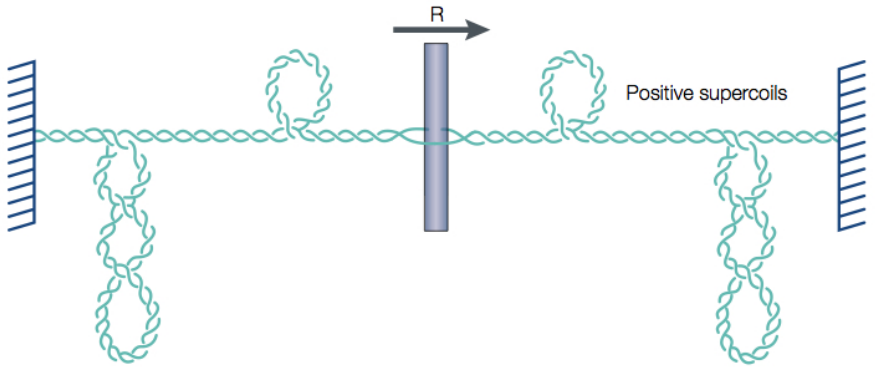

Figure 2.5: The twin-supercoiled domain at the replication site. When the replication complex processes through the DNA double helix positive supercoils forms in front and negative supercoils forms behind it when the helix is restricted from rotating while the complex is restricted from rotating around the helical axis. [46].

Topoisomerase in gene expression.

When the mechanisms of the different types of topoisomerases are compared to the gene expression mechanisms, the conclusion is that topoisomerase IB and topoisomerase II can operate in front of the replisome to reduce positive supercoils. At the end of a replication process the two replication forks meet and the synthesized strands will be intertwined. Hence the double helix strand passage mechanism of topoisomerase II is needed to decatenate the two strands in order for the chromosome to segregate. In transcription only a small part of the double helix is open at a time, contrary to replication where the unwinded part of the double helix grows. This means that the degree of supercoiling should be balanced in transcription, instead of just released as in replication. This balance can be held by the gyrase which can remove posive supercoils (introduce negative) and topoisomerase IA which can remove negative supercoils. A certain degree of negative supercoils facilitates the opening of the double helix and initiates, e.g., transcription. If too high a degree of negative supercoils arises behind the transcription complex, it causes the double helix to destabilize and unwind. The bases of the mRNA transcript can then form pairs with the bases in a DNA strand, forming a structure called a R-loop [46]. Such formation prevent the translation of mRNA and stall protein synthesis. The role of topoisomerase I and gyrase is therefore important for cell survival.

Chapter 3

Tethered Particle Motion (TPM)

The tethered particle motion (TPM) technique depends on the restricted Brownian motion of a particle as seen in figure 3.1. Information about the conformational change of the tether is obtained by observing the particle motion. In that way the particle, often referred to as a bead, is used as a probe to test a biological system such as DNA-protein interaction. A DNA molecule would in that case be the tether. When the protein interacts with the DNA, the conformational changes cause an overall change in tether length, reflected by a change in particle motion.

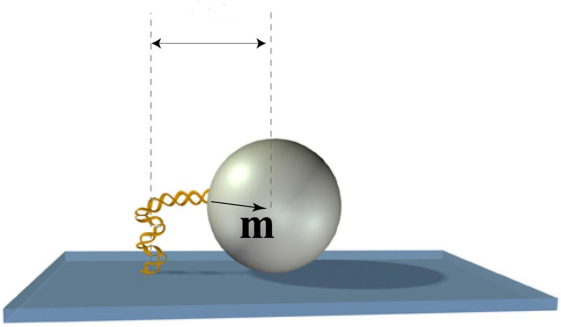

Figure 3.1: A bead tethered to a surface by a DNA molecule similar to the system used in the present work but with the difference that the DNA molecule was a supercoiled plasmid. [29].

3.1 Theoretical view of TPM

The probe's motion is related to Brownian motion: the random drift of particles suspended in a liquid. If the motion is considered in a series of time steps, the displacement in each

step would be the sum of a random component and a deterministic component arising from the drift towards a tether's anchor point [8]. The motion is therefore a restricted Brownian motion.

Brownian motion.

The "pure" Brownian motion of particles can be considered random in that sense that a particle forgets its previous steps and moves independently of other particles. The displacement is therefore a stochastic process. It arises from the enormous amounts of collisions with water molecules in each step. The probability distribution for a Brownian particle follows the diffusion equation:

$$\frac{\partial P(x,t)}{\partial t} = \frac{\partial^2 P(x,t)}{\partial x^2} \tag{3.1}$$

and has the solution:

$$P(x,t) = \frac{1}{4\pi Dt} e^{\frac{x^2}{4Dt}} \tag{3.2}$$

for start position at 0 and a start time 0. Equation (3.2) is a normal distribution and the mean is given by the first moment: $\langle x(t) \rangle = \int_{-\infty}^{+\infty} xP(x,t)dx$ and the variance by the second central moment: $\langle x(t)^2 \rangle - \langle x(t) \rangle^2$. The mean is 0 and the variance is

$$\langle x^2 \rangle = 2Dt, \tag{3.3}$$

where $\langle x^2 \rangle$ is the mean squared displacement in one dimension. D is the diffusion coefficient which is dependent of water temperature, water viscosity, and particle size. In the Stoke-Einstein relation D for a sphere is given by

$$D = \frac{k_b T}{6\pi\eta r}, \tag{3.4}$$

where k_b is the Boltzmann constant, T the temperature, η the viscosity and r the radius. The same distribution can be reached from a random walk model (in one dimension) where the probability to step right or left is $1/2$. A binomial can describe this probability and when the number of steps goes to infinity and the probability of taking a step remains constant, the binomial is approximated by the Gaussian function.
From the displacement equation (3.3) it can be seen that the time, t, scales with the square of the distance, $\langle x^2 \rangle$. This means that walking twice a distance takes 4 times as long and walking 10 times a distance takes 100 times as long. This has a characteristic impact on the trace of a walking particle which may not seem very intuitive at first. Imagine taking a closer look on a region that a particle walks. The observed particle trace will often cross itself and return to positions it has already visited. This is because small regions are more frequently visited than larger regions. When zooming out the frequently visited regions will appear as clusters and in this large view the particle does not tend to visit all available sites. It looks as if the particle likes to explore some regions while neglecting others. This behavior is shown in figure 3.2. It does not distribute its visits evenly. If it did so it would not be an independent random walk. The independence arises from the fact that the steps are considered on a timescale, Δt, much longer than the time it takes a particle to change velocity, which is referred to as the correlation time, τ_c. When $\Delta t >> \tau_c$ the steps are independent and the sum of them will be Gaussian distributed in accordance with the central limit theorem.

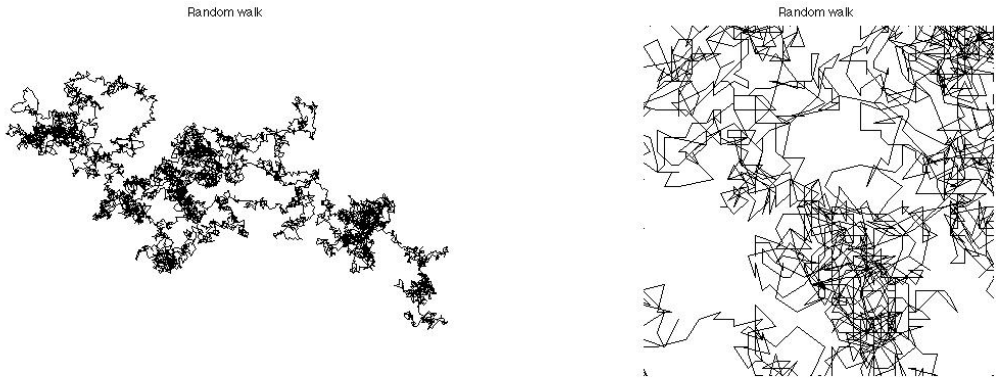

(a) (b)

Figure 3.2: Simulated random walks of 10000 steps. (a) Full view. (b) Zoomed view (but on another simulated walk).

DNA – a biopolymer.

In TPM the bead is often tethered by a DNA molecule which is also the case for the experimental work in this thesis. The DNA molecule is considered a polymer. A polymer consist of a number of repetitive units chemically bound to constitute a chain. Its statistical properties is therefore described on the basis of this chain-like nature.
If the chain is considered flexible with the subunits free to rotate relative to each other the conformation can be approximated as a random walk with n steps of length l. The conformation is dependent on the trajectory of the random walk and so to quantify the conformation the end-to-end distance of the polymer, R, is used. The steps are uncorrelated and R is the sum of random variables and hence described by a Gaussian distribution:

$$P(R,n) = \Big(\frac{3}{2\pi n l^2}\Big)^{3/2} \exp\Big(-\frac{3R^2}{2nl^2}\Big). \tag{3.5}$$

This distribution describes an ideal chain and does not account for the space already occupied of the chain which hence is inaccessible and called the excluded volume. The exclusion of not accessible conformations causes the mean square end-to-end distance of the polymer, $\langle R^2 \rangle$, to be larger than approximated here. In the same way a bead tethered by a polymer close to the surface would also be excluded from volumes near the surface. The effect is an entropic force driving the conformation of the chain away from the most probable (with highest entropy) state. Whether the motion is dominated by the bead or the polymer can be expressed in terms of the excursion number N_R [38]. The bead dominates if

$$N_R = \frac{R}{\sqrt{\frac{l_0 \xi}{3}}} > 1, \tag{3.6}$$

where R is the bead radius, l_0 is the contour length, and ξ is the persistence length. The persistence length quantifies the stiffness of a polymer. If two vectors is situated a distance L from each other on a polymer then the expectation value of cosine to the angle, θ, between them is given by

$$\langle \theta \rangle = \exp -(\tfrac{L}{\xi}). \tag{3.7}$$

The correlation between the $\langle\theta\rangle$ and the distance L falls exponentially with the increase in distance. The stiffer the polymer the longer the characteristic distance for the correlation becomes and the larger the persistence length must be. If the polymer is shorter than its persistence length it behaves as a stiff rod. If the polymer is longer than the persistence length it must be modeled as a chain of stiff rods situated relative to each other statistically described by a Gaussian distribution. The persistence length of DNA depends on the ionic environment but is approximately 41 nm in a buffer[1] similar to the one used in this study [47].
N_R for a DNA molecule of 1300 nm tethered to a bead with radius of 250 nm is approximately: $N_R = 1.9$. The plasmid used in the topoisomerase experiments is 7600 bp and circular. If it is fully stretch but still in the closed form it would make a tether of ~ 1300 nm (conversion factor: $0.34^{nm}/_{bp}$). The plasmid is supercoiled and not fully stretched and so N_R will always be larger than estimated here. The bead should therefore always dominate the motion.
A bead tethered by a DNA molecule can be considered attached to a spring. The force exerted from the DNA molecule is entropic in origin (it tends to maximize its entropy). With the use of the probability density function 3.5 the entropy is given as

$$S = k_b \cdot ln(P(R)). \tag{3.8}$$

The stretching force acting on the spring is given by

$$F = \frac{3}{2}\frac{k_b T}{\xi}\frac{x}{l_0}, \tag{3.9}$$

where F is the force, K_b the Boltzmann constant, T the temperature, ξ the persistence length, x the extension, and l_0 is the contour length [39]. This is the Worm-Like Chain model in a very low force regime. In a higher force regime a modified version must be used given by

$$F = \frac{1}{4}\frac{k_b T}{\xi}\Big[\Big(1 - \frac{x}{l_0}\Big)^{-2} - 1\Big], \tag{3.10}$$

as modeled by Marko and Siggia [26, 47].

[1]Buffer: 20 mM Tris, 130 mM K^+, 4 mM Mg^{2+}.

Restricted Brownian motion.

A tethered bead experience not only the random forces from water molecules leading to brownian motion but also a hard wall repulsive force from the surface and a tension force from the tether as given by equation (3.9) [8].
The tether tension inflicts on the bead motion which can no longer only be considered with the mean square displacement component from equation (3.3) but also have a "restricting" component from the tether. The restricted brownian motion will still be Gaussian when modeled. That this is not entirely in accordance with experimental observations can be seen in the chapter 6.

Chapter 4

Experimental Protocol

In the following the experimental procedures and initial results including an electrophoresis gel for testing enzyme activity, are described. The experimental procedures were passed on to me by Kamilla Nørregaard and Stanley Brown [32]. The detailed information about buffer contents, material suppliers and special preparation steps can be found in the appendix A.

4.1 Experimental bioassay

To get a stable tethered bead persistent to flow forces, the assay was assembled using high-affinity biomolecules and peptide nucleic acids (PNAs). The complete bioassay was assembled as

surface-antidigoxigenin-digoxigenin-PNA-plasmid-PNA-biotin-streptavidin-bead

and can be seen in figure 4.1. Via a biotin conjugated PNA the plasmid was attached to a streptavidin coated bead and via a digoxigenin conjugated PNA to an anti-digoxigenin coated surface. The anti-digoxigenin/digoxigenin and biotin/streptavidin handles are commonly used in bioassays to functionalize surfaces. The adaptation of PNA as handles are much more unusual and gives the possibility to tether a plasmid and have the advantage of strengthen the tether as described next.

Site specifity and robust handles through PNA.

PNA is similar to DNA and RNA but have a peptide linked backbone of 2-aminoethylglyciens and bases bound by methylenecarbonyls as seen in figure 4.2a.
DNA and RNA have a phosphate-sugar backbone with sugar bound bases, deoxyribose and ribose respectively. The phosphates have a negatively charged group which make two strands repulsive to each other and weakens the attractive hydrogen bonds between

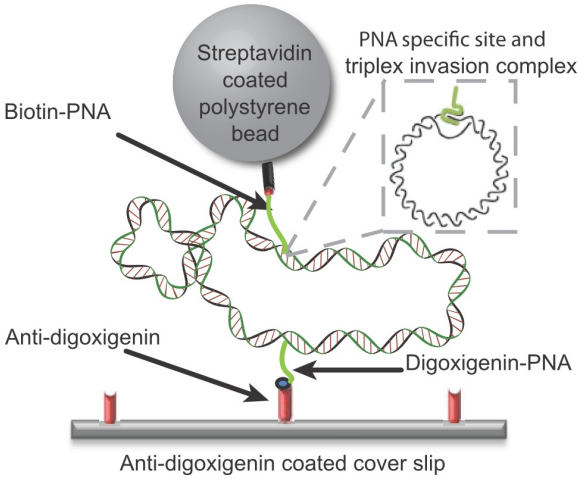

Figure 4.1: The bioassay. A streptavidin coated microsphere is attached to a plasmid through a biotin-PNA handle. The plasmid is attached to a anti-digoxigenin coated surface by a PNA-digoxigenin handle. The figure was kindly provided by Kamilla Nørregaard.

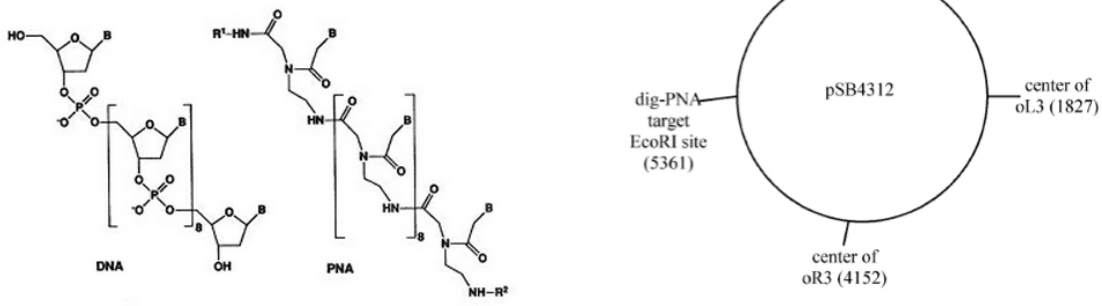

(a) (b)

Figure 4.2: (a) The chemical structures of DNA and PNA [30]. (b) Schematic of the *E. coli* plasmid. The target sites for PNA strand invasion is indicated by base pair numbers. They are placed asymmetrically on the plasmid.

the corresponding bases. PNA lack this negatively charged backbone as its peptide backbone is neutral and therefore is binds more strongly than DNA and RNA. Accordingly a PNA/DNA duplex is also favored over the single component duplex because it has a higher stability. Furthermore the PNA are site specific as it consists of the complementary bases to the DNA strand it binds to. Thus a handle can strategically be placed in a plasmid through the design of the PNA sequence so it match a DNA sequence. PNA binds to the double helix by strand displacement and a triplex structure is formed as illustrated in the figure 4.1 inset [30].

Plasmid construct.

The plasmid used is sketched in figure 4.2b. The sites for PNA annealing are marked and given in base pair numbers. Notice they are asymmetrical situated to each other. This is not intended as part of the experiment but simply an instance of reusing a bioassay designed to Kamilla Nøregaard's thesis. This bioassay had proven stable in tether formation and was therefore adopted in the present project. The slightly asymmetrical placement of the handles was earlier shown to have a negligible impact of the symmetry for a tethered bead's motion using bead sizes similar to the ones used in the present work [32]. The asymmetrical placement of the handles are therefore of no significance.
It was found that 90 % of the plasmids had at least one supercoil. Kamilla Nørregaard made a chloroquine gel electrophoresis to obtain the supercoiling distribution for the plasmid used in both her and in the present project. The distribution showed the presence of 10–15 different states of supercoiling. The difference in the number of supercoils between states was not analyzed, only the number of states [32]. The precise supercoiled state of a plasmid tether in an experiment is hence not known.

4.2 TPM procedure

The TPM takes place in a flow chamber. Inside the chamber the beads have been attached to the surface through tethers like a ship anchored to the bottom of the sea. Hence the polystyrene beads are restricted in their Brownian motion and the motion of individual beads is recorded through a microscope and analyzed both with and without the presence of topoisomerase.

Preparation of a flow chamber.

The flow chamber is build by sandwiching a glass slide and a thin glass cover slid with spacers of Parafilm as illustrated in figure 4.3. The glass should be gently wiped with lens paper to clean it. (By experience it seems preferable not to clean in alcohol as it makes the

spacers less "sticky" and the chamber less resistible to leaking). Two spacers of Parafilm are cut and placed parallel to each other along the edges of the cover slide. The cover slip is put on top to form a closed chamber. The chamber is heated at 120 C° in 30 seconds until the Parafilm is melted. When cooled down the Parafilm will glue the chamber together. While the chamber is heating a gentle push on the top with a stick or mechanical tweezer will fix the slit in the Parafilm. The push should be in a center-to-edge movement to get rid of air bubbles forming between the Parafilm and glass surface. Lastly, the excess Parafilm is cut loose to get a fine Parafilm-glass edge at the ends of the chamber. In that way the fluid is prevented from running between the spacer and glass surface and disassemble the chamber. I prepared chambers of approximately 20 μl in volume.

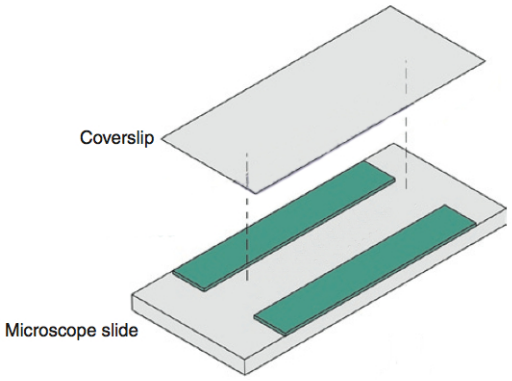

Figure 4.3: A flow chamber with Parafilm spacers.

Functionalization of the surface.

The TPM sample is prepared in steps starting with 1) coating of the glass surface with anti-digoxigenin, 2) blocking the rest of the glass surface with α-Casein , 3) adding the plasmid tethers in low concentration in order to get single tethered beads, and 4) adding the beads. The 5) and last step of adding topoisomerase happens only after the tethered beads have been successfully observed and recorded for a short period of time in the microscope. The incubation and washing buffers, PBS and λ-b (se appendix A), are introduced into the chamber by capillary forces. Once the chamber is filled the buffer can be exchanged by sucking out solution in one end while introducing new solution at the other from a pipette. To minimize the evaporation of buffer during the incubation period the sample is placed above a small amount of water in a closed box. Furthermore, it is important to leave a small droplet at each edge of the chamber as a kind of buffer reservoir which will prevent

the sample chamber to dry out. The preparation steps takes place in room temperature and are as follows:

1) 20 μl PBS with 20 μg μl anti-digoxigenin incubates for 30 min. The chamber is then washed with 90 μl λ-b+DTT.

2) 20 μl λ-b with 2 mg/ml α-Casein incubates for 30 min. Washed with 90 μl λ-b+DTT.

3) 20 μl λ-b with 2 pM plasmid incubates for 60 min. Washed with 90 μl λ-b+DTT.
The PNA handles are annealed to the plasmid before the plasmid is used for the sample preparation. This is done by incubating a mix of plasmid with PNA at 37°C for minimum 15 hours. Before use the construct is diluted in λ-b and heated to 60°C for 10 min to removed unspecific bindings. When cooled to room temperature the construct is ready for use.

4) 20 μl PBS with 0.02 ‰ w/v streptavidin coated polystyrene beads 0.46 μm in diameter incubates for 30 min. Washed with 90 μl λ-b+DTT.
The beads from the supplier are washed and kept in PBS. Before use 2 mg/ml α-Casein is added to the bead solution to prevent the beads from aggregating and the solution is sonicated for a minimum of 15 minutes to dissolve possible formed agglomerates.
A tethered bead is observed for a period of time in the enzyme free environment. Then the topoisomerase is introduced very gently while the sample is mounted in the microscope.

5) 20 μl reaction buffer with 0.125 units/μl topoisomerase is flushed into the chamber. 1 unit is defined as the amount of enzyme that catalyzes >95% of 0.5 μg of DNA (plasmid cloning vector pUC19 of replicative form I) in a 25 μl reaction volume in 15 min at 37 C°.

It is important to work with very clean buffers and to maintain the sample clean, to get tethered particles. Therefore, all buffers were filtered with a gel Ficoll filter from GE Healtcare. Samples made with filtered versus non-filtered buffers showed a clear difference in purity and amounts of successful tethers.

Reaction buffers.

The reaction buffers used in experiments with topoisomerase IA and IB are in general consistent when comparing papers from the literature. A comparison can be seen for the single molecule experiments made on topoisomerase IA and IB in table 4.1 where also the reaction buffer provided by New England Biolab (NEB) is listed. The experiments carried out in the present thesis were performed in a modified version of the NEB buffer as it turned out that tethers had a tendency to collapse in the NEB buffer. In addition a high ion concentration is desirable to get a large change in bead motion from a supercoiled to

a relaxed plasmid (more on this in results chapter 6). The modified version, abbreviated MB, is also listed in the table. The first three constituents, Tris-acetate, EDTA, and KCl form the λ-buffer also used in the preparation procedure. The concentrations of topoisomerase used (listed as enzyme in the table) is hard to directly compare as the units are different. But considering the definition of a unit the amount of DNA that one unit of topoisomerase relaxes is ~ 10 nM (the pUC19 has a molecular weight of 1750 kDA) in 25 μl. Then the amount of 0.125 u used in the experiments should by far exceed the necessary concentration of topoisomerase defined by the dissociation constant $K_d = 200$ pM [16].

Topoisomerase IA	Topoisomerase IB	NEB	MB
50 mM Tris·HCl	10 mM Tris·HCl	20 mM Tris-acetate	10 mM Tris-acetate
120 mM NaCl	50 nM NaCl	–	0.1 mM EDTA
10 mM KCl	–	50 mM K-acetate	200 mM KCl
3 mM $MgCl_2$ (0.25 mM)[†]	10 mM $MgCl_2$ (2 mM)[‡]	10 mM Mg-acetate	2 mM MgCl
1 mM dithiothreitol	1 mM dithiothreitol	1 mM dithiothreitol	1 mM dithiothreitol
200 μg/ml BSA	200 μg/ml BSA	100 μg/ml BSA	100 μg/ml BSA
380 pM enzyme	0.5 – 20 nM enzyme	–	0.125 units [II]
–	–	25 °C	room temp.

[†] Concentration used to slow down enzyme reaction in order so see stepwise activity.
[‡] Concentration used to measure DNA rotation rate in enzyme cavity.
[II] The definition of one unit is given in the subsection *Functionalization of the surface* in the present section 4.2.

Table 4.1: Reaction buffer substances and concentrations used in the studies of topoisomerase IA [16] and IB [21] and also for the buffer provided by NEB. Acetate is the group -$OOCCH_3$.

Experimental recordings.

Equipment. Images were recorded with the software ParaSequencer (Parameter AB, Sweden) via a high speed progressive scan camera (Pike F-100B, Allied vision technology, USA) on an inverted microscope (Leica model DM IRB, Switzerland) with a 63x water objective $NA = 1.2$ (Leica) and a 1.6x zoom (Leica).

Data acquisition. Timeseries for bead motion parallel to the surface in the image plane (the (x,y)-plane) was recorded. The recorded image field was 62x62 pixels and the frame rate was 225 frames per second. The ParaSequncer output was an image file (an AVI file) and a text file with corresponding numbers of frames recorded. These were first analysed with a LabVIEW bead tracking program (St. Andrew Tracker [28]) and the output was a text file containing x- and y-positions for each image frame. The position data was then analyzed in Matlab. The conversion from pixel to nm had been made earlier[32]. A surface

stuck bead was moved with a piezo from which the distance was known and correlated with recorded images of the displacement. The conversion factor was 45.97 nm/pixel.
A flow chamber was mounted and observed in bright field microscopy mode. Through visual inspection a tethered bead candidate was found. It was possible to tell a tethered bead from a non-tethered bead by observing the motion for a short period. Tethered beads showed a clear restricted motion compared to non-tethered beads. The focus was adjusted to get a high contrast between the tethered bead and background. Recordings were made for about 16 minutes for each bead in intervals of 1, 2, or 4 minutes to reduce movie file size and hence processing time in the bead tracking analyse. Each processed movie was catenated in the Matlab data analysis to get a complete time series.

4.3 Gel electrophoresis

It is the negatively charged backbone which makes DNA migrate in gel electrophoresis. When voltage is applied DNA fragments of different size can be separated. The gel porosity also influences the separation and DNA fragments with different topology can be separated. In an agarose gel supercoiled plasmids will migrate further than relaxed and linearized ones. The supercoiled plasmids take up less space and their mobility are enhanced.

Testing topoisomerase activity.

To see whether the enzyme was active gel electrophoresis was performed. Stanley Brown assisted the work by making the agarose gel, electrophoresis buffer, and loading buffer.

Materials. The gel electrophoresis was performed in 0.8 % agarose with tris-acetate EDTA (TAE) electrophoresis buffer at 100 V, 6 W, 200 vol·hrs. The loading buffer contained 20 % Ficoll as density agent, bromophenol blue as marker dye and 0.1 M EDTA as enzymatic stop agent [40, 20]. The reaction was tested in a reaction buffer provided by NEB containing 20 mM tris-acetate, 50 mM potassium acetate, 10 mM magnesium acetate, 1mM dithiotreitol and 100 μg/ml BSA. The topoisomerase activity was also tested in a modified version of the reaction buffer (MB) which contained 10 mM tris-acetate, 200 mM potassium chloride, 2 mM magnesium chloride, 1 mM dithiotreitol and 100 μg/ml BSA in λ-b. The samples were tested at room temperature.

Method. The enzymatic activity was tested on the plasmids as function of time, concentration and buffer. The different samples are listed in figure 4.4 and table 4.2 where the values succeeding the sample names give the reaction time. Plasmids, reaction buffer and topoisomerase were mixed and the loading buffer was added to stop the reaction. The first sample is without topoisomerase (w/o) and the second is with a 10 time dilution of

topoisomerase (0.1x). 2 μg plasmid and 2 units topoisomerase were used for a reaction volume of 30 μl in which the loading buffer was added 1:4. 2 μl and 10 μl samples were loaded from each of these 40 μl sample volumes onto the gel. The stained gel result can be seen in figure 4.4. The lanes alternately holds 2 μl and 10 μl such that lane 1 corresponds to a 2 μl sample and lane 2 to a 10 μl sample and so forth.

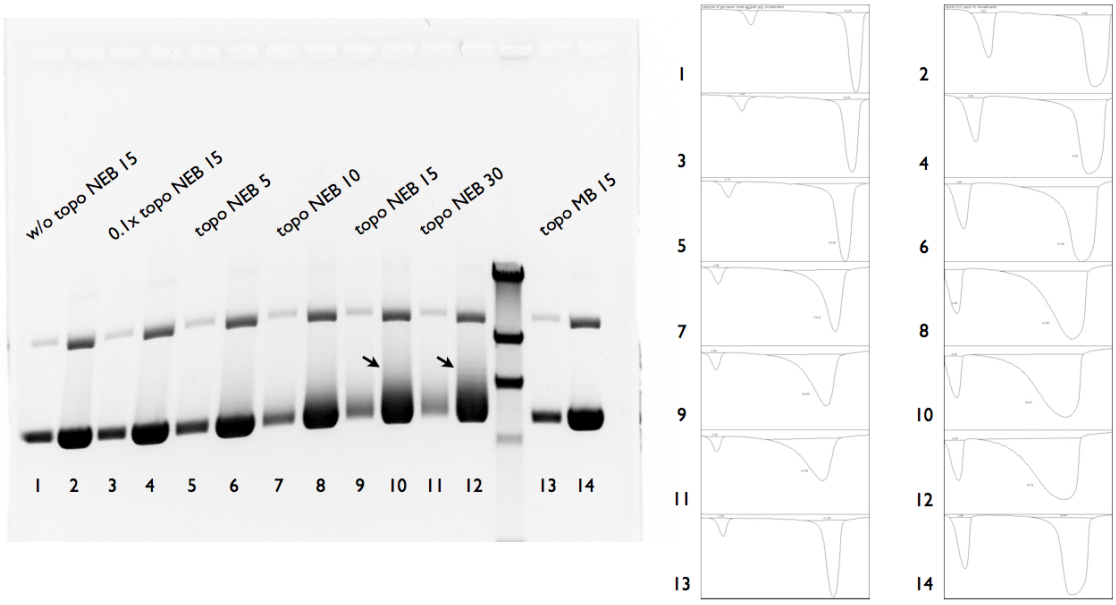

Figure 4.4: The stained gel and the corresponding intensity profiles for the 2 μl and 10 μl lanes. Match in numbers correlate the lanes and profiles. Arrows indicate plasmids of different supercoiling degrees. Enlarged profiles can be viewed in appendix B.1.

Results. The plasmids ran in the direction from top to bottom in the picture in figure 4.4. From a quick visual inspection it can be seen that a large amount of plasmids occupy the bands that ran the longest distance. This is the supercoiled plasmids. If the test lane, w/o topo NEB 15, with no topoisomerase present is compared with the other lanes, it is seen that the other lanes are less sharply defined and appear more smeared out. The longer period topoisomerase was active, the more smeared out the lanes are. The topoisomerase is therefore active and resolves more and more supercoils the longer time it is active. The more relaxed the plasmids become the shorter distance they travel indicated by the smeared bands. At a closer look plasmids with different degrees of supercoiling can also be distinguished through the migrated bands. This is indicated with arrows in the lanes topo NEB 15 and topo NEB 30. Normally a chloroquine gel is used to get a better resolution

of supercoiling degree but in the present case a positive/negative test of enzyme activity was sufficient.
The activity can be quantified from the intensity of the bands (which represents the density of plasmid). The intensity profiles can be seen in figure 4.4 right. The areas of the peaks represent the relative intensity to each other. The areas are quantified using the ImageJ gel analyzer tool. A baseline was chosen for each peak before the areas were calculated. The quantified values are given in table 4.2. The final bands value of MB 15 relative to w/o topo 15 is 1.20 and indicates that the topoisomerase is active also in the modified buffer which can be hard to tell from just the visual inspection of the gel where lane 2 and 14 looks similar. The relative value for NEB 15 to w/o topo 15 is 1.75. The higher value for the reaction in a buffer from NEB indicates that the topoisomerase works best in the provided buffer from the supplier (NEB).
The gel seems very saturated which means that the calculated density percentage could be a bit off. At a certain saturation level one can no longer measure an increase in density. The density seems a little less on the 2 μl lanes. The relative values for the final bands for the 2 μl lanes is given in the appendix table B.1. The values for w/o topo 15, MB 15 and NEB 15, (lane 1, 13 and 7) is: $1 : 1.01 : 1.32$. This is a much lower level compared to the 10 μl lanes, which was $1 : 1.20 : 1.75$, but it shares the same tendency: that the bands are smeared out the longer the topoisomerase has been active and that the activity is higher in NEB buffer. The quantified values are therefore maybe not to be trusted for their exact values but they prove that topoisomerase is active under the experimental conditions at room temperature. The complete tables of quantified values for the gel together with the intensity profiles can be viewed in the appendix B.1.

sample	band	% area	$r_{w/o\ topo}$	$r_{fin/ini}$
w/o $topo_{15}$	ini	2.816	1	2.98
w/o $topo_{15}$	fin	8.38	1	
0.1x $topo_{15}$	ini	2.80	0.99	3.41
0.1x $topo_{15}$	fin	9.55	1.14	
NEB_5	ini	2.88	1.02	3.82
NEB_5	fin	11.02	1.31	
NEB_{10}	ini	2.68	0.95	4.77
NEB_{10}	fin	12.81	1.53	
NEB_{15}	ini	2.45	0.87	5.98
NEB_{15}	fin	14.67	1.75	
NEB_{30}	ini	2.28	0.81	6.44
NEB_{30}	fin	14.71	1.75	
MB_{15}	ini	2.94	1.04	3.41
MB_{15}	fin	10.02	1.20	

Table 4.2: Results for 10 μl lanes. The samples correspond the lanes in figure 4.4 and the subscripts give the reaction time. Each lane has an initial and final band in the top and bottom respectively as seen in figure 4.4. % area is to the area of the total area under all profiles together. $r_{w/o\ topo}$ indicates the value relative to the sample w/o topoisomerase and is calculated as the ratio between two % area values. $r_{fin/ini}$ gives the % value for the initial band relative to the final band.

Chapter 5

TPM Analysis

The quantification of tethered bead motion involves a bead tracking algorithm and a visualization of bead position data. The bead tracking algorithm outputs sub-pixel resolution position data.

5.1 Bead tracking

Bead tracking algorithm based on the cross correlation method.

There are several methods for tracking single particles such as The Centroid (center of mass), The Gaussian Fit, The Sum-Absolute Difference, and The Cross Correlation [13]. The particle tracking method used in this project is based on cross correlation. The algorithm is named The St. Andrews Tracker and is a LabVIEW based software made by Graham Milne [27]. The software relies on a template matching technique: on the basis of a template image the software searches consecutive images for matching patterns [28]. A bead appearing in the template will be recognized in the following images and the bead's center position, (x, y), will be stored for each image. The algorithm includes a normalized cross correlation method used for the pattern matching (in a modified version reducing the computation time). Each image is represented by a matrix holding, e.g, values for the intensity and each matrix entry, (i, j), corresponds to a pixel. The best match between a template image and a consecutive image is found by calculating the sum of the products of every entry between the two image matrices. The sums form the cross correlation matrix. Imagine two overlapping images both with a dark spot representing a bead. If one image is moved relative to the other the sum of the product of their matrix entries will grow as the spots are overlapping and reach a maximum when the spots completely overlaps. The largest value in the cross correlation matrix is this maximum. The cross correlation matrix, $\mathbf{C}$, can be defined as

$$\mathbf{C}_{x,y} = \sum_{i=0}^{n-1} \sum_{j=0}^{m-1} \mathbf{T}_{x+i,y+j} \mathbf{I}_{i,j}, \tag{5.1}$$

where $\mathbf{T}$ is the template matrix and $\mathbf{I}$ the consecutive image matrix. The calculation is running trough the entries of both matrices via i and j one image, (x, y), at a time. When every image has been compared to the template, each maximum of the cross correlation matrices form the history of bead positions.
The method has a tendency of matching the brightest/darkest regions of two images which not necessarily gives the best topological correlation. This tendency can be alleviated by normalizing with the root mean square (RMS) [13]. A relative offset in intensity between the template and a consecutive image can be dealt with by subtracting the mean from each intensity value [13]. Imagine intensity values for an image which decreases because of an offset (the baseline decreases). When correlated with another image the decreasing values will "drag down" the correlation values. This means that the real correlation maximum value could be downshifted to an extend that it is no longer the maximum value. To correct for this the intensity offset is therefore important. The normalized form of $\mathbf{C}$ is defined as

$$\mathbf{C}_{x,y} = \frac{\sum_{i=0}^{n-1} \sum_{j=0}^{m-1} \left[\mathbf{T}_{x+i,y+j} - \bar{\mathbf{T}}_{x,y}\right] \left[\mathbf{I}_{i,j} - \bar{\mathbf{I}}\right]}{\sqrt{\sum_{i=0}^{n-1} \sum_{j=0}^{m-1} \left[\mathbf{T}_{x+i,y+j}\right]^2} \sqrt{\sum_{i=0}^{n-1} \sum_{j=0}^{m-1} \left[\mathbf{I}_{i,j}\right]^2}}, \tag{5.2}$$

where the denominator holds the RMSs and the mean matrices are given by

$$\bar{\mathbf{T}}_{x,y} = \frac{1}{n \cdot m} \sum_{i=0}^{n-1} \sum_{j=0}^{m-1} \mathbf{T}_{x+i,y+j} \qquad \bar{\mathbf{I}} = \frac{1}{n \cdot m} \sum_{i=0}^{n-1} \sum_{j=0}^{m-1} \mathbf{I}_{i,j}. \tag{5.3}$$

Sub-pixel resolution with paraboloid interpolation based on least square approximation

Because each entry in the matrices corresponds to a pixel the resolution of the position described above is a whole pixel size. To get sub-pixel resolution a paraboloid surface is fitted to values of the correlation matrix $\mathbf{C}$ and through interpolation the maximum,

(x_{max}, y_{max}), is found [13]. The general equation for a 2D paraboloid is given by

$$z(x, y) = ax^2 + by^2 + cx + dy + e. \tag{5.4}$$

The interpolation is made from the pixel containing the largest correlation value and the four surrounding pixel values. Using these pixel values the paraboloid coefficients can be found: the five pixels gives us five positions which substituted into the paraboloid equation gives us a set of five equations with five unknown coefficients. The first equation using the central pixel position would be: $z_1 = z(x_0, y_0) = ax_0^2 + by_0^2 + cx_0 + dy_0 + e$, the second using the pixel right to the center pixel (seen from above) $z_2 = z(x_1, y_0) = ax_1^2 + by_0^2 + cx_1 + dy_0 + e$. To find the coefficients so that the paraboloid equation best fit all five points we must solve the system of five equations. In shortened notation:

$$\begin{bmatrix} x^2 & y^2 & x & y & 1 \\ \vdots & \vdots & \vdots & \vdots & \vdots \end{bmatrix} \begin{bmatrix} a \\ \vdots \end{bmatrix} = \begin{bmatrix} z_1 \\ \vdots \end{bmatrix}. \tag{5.5}$$

In general: if we try to fit more points than coefficients (more equations than unknown coefficients) the system can be solved using *normal equations* which yield the *least square* approximations. In other words: there is no exact solution to the system because the points does not lie exactly on a paraboloid but we can find approximated values from the normal equations. The system of equations and the corresponding system of normal equations are denoted as

$$\mathbf{Ac} = \mathbf{z} \qquad \mathbf{A^T Ac} = \mathbf{A^T z}, \tag{5.6}$$

where $\mathbf{A}$ would be equivalent to the variables, $\mathbf{c}$ to the unknown coefficients and $\mathbf{z}$ to the paraboloid values z. $\mathbf{A^T}$ is the transpose of the matrix $\mathbf{A}$. The normal equations can be solved by matrix augmentation (after multiplication with $\mathbf{A^T}$ the new $\mathbf{A}$ and $\mathbf{z}$ are merged) and Gauss elimination. At the end of the Gauss elimination one coefficient is known. By back-substitution the rest of the coefficients are found.Lastly the coefficients defining the paraboloid that best fit the five pixels is left. The maximum of the paraboloid (5.4) is found by the partial derivatives:

$$0 = \frac{\partial z}{\partial x}(x,y) = 2ax + c + e \qquad 0 = \frac{\partial z}{\partial y}(x,y) = 2ay + d + e \tag{5.7}$$

and the maximum and sub-pixel resolved bead position for an image is then given by

$$(x_{max}, y_{max}) = (\frac{-c}{2a}, \frac{-d}{2b}). \tag{5.8}$$

Notice how the coefficients easily can be found for the system when five points are used and the central pixel value are set to 0: $z(x_0, y_0) = (0,0)$ [13]:

$$\begin{aligned} a &= -z(x_0,y_0) + \tfrac{1}{2}z(x_1,y_0) + \tfrac{1}{2}z(x_{-1},y_0) \\ b &= -z(x_0,y_0) + \tfrac{1}{2}z(x_0,y_1) + \tfrac{1}{2}z(x_0,y_{-1}) \\ c &= \tfrac{1}{2}\big(z(x_1,y_0) - z(x_{-1},y_0)\big) \\ d &= \tfrac{1}{2}\big(z(x_0,y_1) - z(x_0,y_{-1})\big) \\ e &= 0. \end{aligned} \tag{5.9}$$

(5.10)

The St. Andrews bead tracking algorithm was tested to have a sub-pixel resolution down to ~ 10 nm [28].

Exposure time vs. diffusion time

In a blurred image the brightest spots are smeared out. This means that the precision with which the bead position is found can be lowered with blurring of the bead. The major contributor of blurring in a TPM setup is the diffusion of the bead. Apparatus movement is slow and spherical aberration are negligible in comparison. In order to decrease the blurring effect caused by bead motion a small image exposure time is used. Furthermore a progressive scan camera is used. The advantage of a progressive scan camera is easiest understood by comparing it to the contrary technique: the interlaced scan. An interlaced image consists of two consecutive recorded image fields, one of even displayed lines and one of odd displayed lines. Put together they form a full frame. The idea is sketched out in figure 5.1. The full frame can therefore be formed with twice the speed and half the

bandwidth (amount of data per time) of that a non-interlaced image would require. But an interlaced frame would be distorted with the time lap between the two fields similar to a blurring effect. This is avoided by using a progressive scan camera which only records one single field image. Furthermore the progressive scan camera used in the present project records at a high speed. A frame rate of 225 frames per second was used. This gives an exposure time < 5 ms. This quantity is sufficiently small compared to the diffusion time as reasoned in the following.

(a) (b)

Figure 5.1: Drawing of interlaced images. (a) A horizontal moving bead. (b) A vertical moving bead [35].

A rough and simple estimate is made of the time it takes the bead to diffuse its range of motion, that is the variance, from the diffusion equation in one dimension: $t = \frac{\langle x^2 \rangle}{2D}$. For a range of 100 nm the time is $t \approx 58$ ms, where $D = 8.568 \cdot 10^{-13}\ \frac{m^2}{s}$ for a bead of radius 250 nm at 20 °C. Since D holds the viscosity, η, and η changes in the close-to-surface regime that the bead is in, it inflicts on the bead diffusion. The influence is negative but is neglected for now. The bead position should be sampled at a faster rate than it takes for it to perform the period, that is moving from its start position and back again. To describe the outer positions the bead should be sampled at least twice in one period. This is in fact the Nyquist sampling theorem which state that the sampling frequency must be twice or above the highest signal frequency: $f_{sam} \geq 2f_{sig}$. The low range at 100 nm yields $f_{sig} \approx 17$ Hz and therefore $f_{sam} \approx 34$ Hz. In this project the camera rate at 225 Hz should therefore be in a safe sampling frequency range. This is in accordance with similar TPM experiments that find a typical time for a bead to traverse its range of motion to be $\sim$50 ms and use an exposure time of 1 ms [29]. Furthermore it is stated that a large exposure time of 40 ms reduces the apparent amplitude of motion by about 20 % when analysed.

5.2 Data visualization

The output of the bead tracking algorithm is position data. The motion of a bead is visualized in a time series with this data. The visualization procedure is illustrated with a

simulated dataset in this section 5.2 to help clarify the data analysis best possible.

Visualizations of bead displacement.

The position data consist of x and y coordinates of the bead center position in the image plane as a function of time t. A scatterplot of a simulated time series for a tethered bead's positions, (x, y), can be seen in figure 5.2a and the corresponding histograms for x and y coordinates in figure 5.2b. The scatterplot serves as a visual inspection that the bead positions are evenly distributed around a 0 point which represents the tether anchor point. If the scatterplot shows anisotropic motion the bead is considered wrongly tethered and the dataset is discarded.

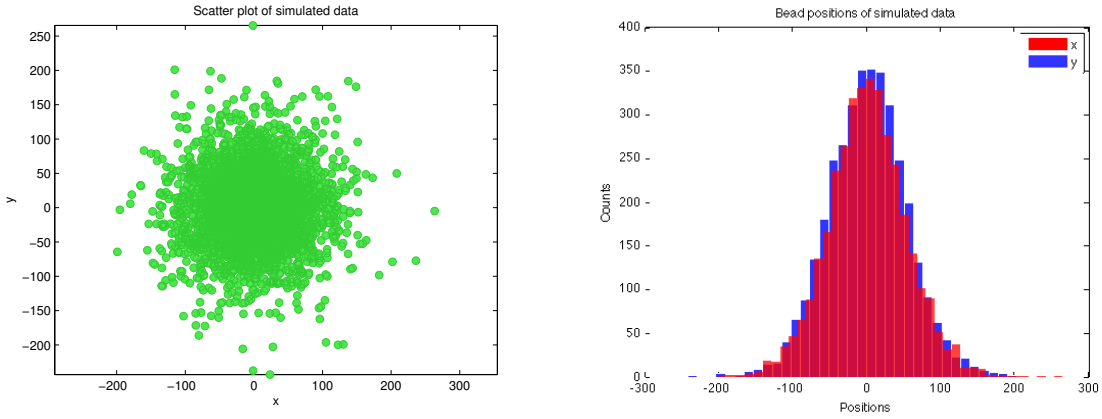

(a) (b)

Figure 5.2: (a) A scatterplot of x and y coordinates for a simulated bead motion. (b) Histograms for the simulated x and y coordinates.

A relaxation of the supercoiled tether reflects in an increase of the effective tether length which again reflects in a larger amplitude of the position fluctuations of the bead. Therefore the amplitude is a measure of a tether extension event. To quantify the amplitude the projected displacement vector of (x, y) is used. This vector will be referred to as the displacement r and is given by

$$r = \sqrt{(x - \bar{x})^2 + (y - \bar{y})^2}, \tag{5.11}$$

where $\bar{x}$ and $\bar{y}$ are the mean positions. The mean values are subtracted x and y in order to reposition the displacement vectors r around the anchor point. This repositioning will

be referred to as a normalization. A time series for the r displacement is shown in figure 5.3a. The displacement r is assessed from the position data shown in figure 5.2. The black trace is the data smoothed by a moving average. The corresponding histograms for r and and r smoothed is shown in figure 5.3b.

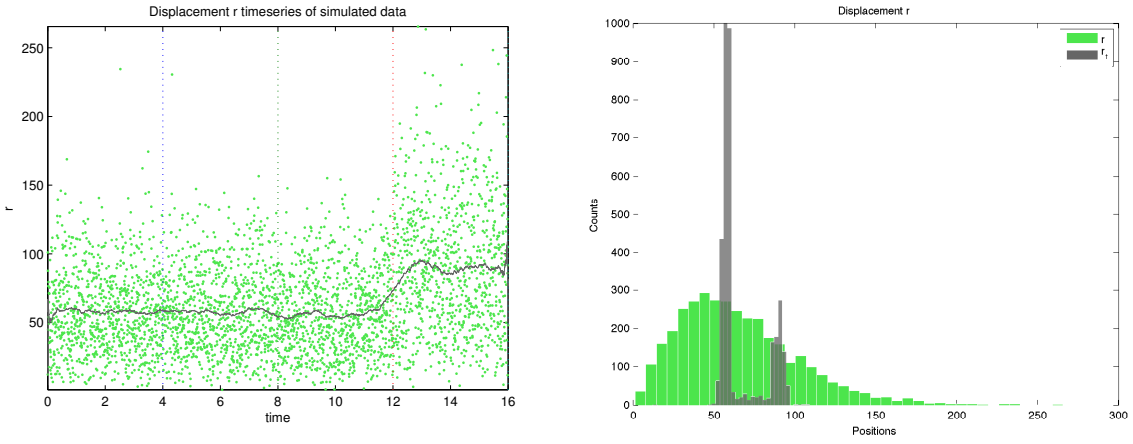

(a) (b)

Figure 5.3: (a) The displacement r time series (grey dots) and the smoothed trace of r made with a moving average (black). (b) The histograms of r and r smoothed.

Simulated dataset

The simulated dataset has one important feature incorporated to resemble real experiments. The last movie has a larger amplitude for the position fluctuations to simulate a tether extension event (a relaxation of the supercoiled tether caused by topoisomerase). The tether extension event can be seen in the time series of displacement r in figure 5.3a in the time range 12–16 and in the last scatterplot (outer right) in figure 5.4. The scatterplots show (x, y) of the individual movies comprising a dataset.

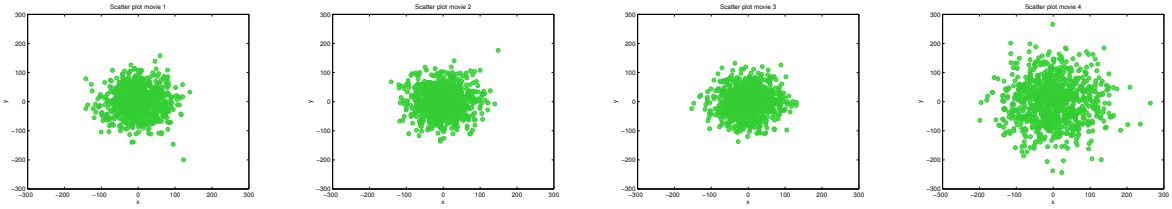

Figure 5.4: Scatterplots of (x, y) for individual movies of a simulated dataset. The last movie (outer right) has a distinct feature of a larger amplitude of bead positions to simulate a tether extension event.

The moving average.

The smoothed traces are made with a moving average filter and help clarify the r displacement because it removes random noise. The filter replaces every data point value, x (the variable x is chosen as an example), with a new mean value: $x \to \bar{x}$. It does so by summing N values in a small window around the particular data point, x, and calculate the mean, $\bar{x}$:

$$\bar{x}(t) = \frac{1}{2N} \sum_{i=-(N-1)}^{(N-1)} x(t-i). \tag{5.12}$$

The mean is calculated at every time t and is hence a moving average. The size of the window can be defined as a time range and will be referred to by τ. The smoothed displacement is referred to as $r|_\tau$ and is then:

$$r|_\tau = \sqrt{\langle (x(t) - \bar{x})^2 + (y(t) - \bar{y})^2 \rangle_\tau}. \tag{5.13}$$

The degree of smoothness comes from the size of τ. Notice from the histograms in figure 5.3b how the change in displacement r emerge as two distributions when the noise is filtered away with the moving average. $r|_\tau$ hence becomes a good quantity of visualizing a tether extension event. The degree of smoothness was set to $\tau = 1$ s.

Shift correction of position data.

A dataset was recorded as a sequence of short movies. This is partly to keep each time series within an acceptable level of minimal drift [32] and to reduce data processing time in the LabVIEW bead tracking program. A dataset of one tethered bead's motion is therefore concatenated from several movies. The points of concatenation in a time series are indicated with vertical lines as seen in figure 5.3a. The LabVIEW program will set a tether anchor point based on the position of the bead in the first image of a movie (the template image). The anchor point will therefore differ among movies comprising a dataset. The result is a time series of movies shifted relative to one another as illustrated in figure 5.5. The upper left shows (x, t) which have been normalized with the mean of all movies. In the upper right (x, t) has been normalized every movie apart. The shifts in tether anchor points among movies require the normalizing procedure used in the upper right figure in order to be corrected. The displacement r defined in (5.11) then becomes

$$r|_\tau = \sqrt{(x(t) - \bar{x}_{movie})^2 + (y(t) - \bar{y}_{movie})^2}, \tag{5.14}$$

where $\bar{x}_{movie}$ and $\bar{y}_{movie}$ represents the normalization per movie. The correct normalization was used to produce the time series of the displacement r shown in figure 5.3a and the incorrect normalization was used in figure 5.5 lower right. Notice how the tether extension event is "hidden" in the time range 12–16 for the time series produced with the incorrect normalization.
This mention of how position data is shift corrected is important to be aware of in the data analysis but can be thought of as a preliminary step in the visualization. Therefore when the displacement r is mentioned one can just consider r as given in (5.11) (otherwise it will specifically be pointed out).

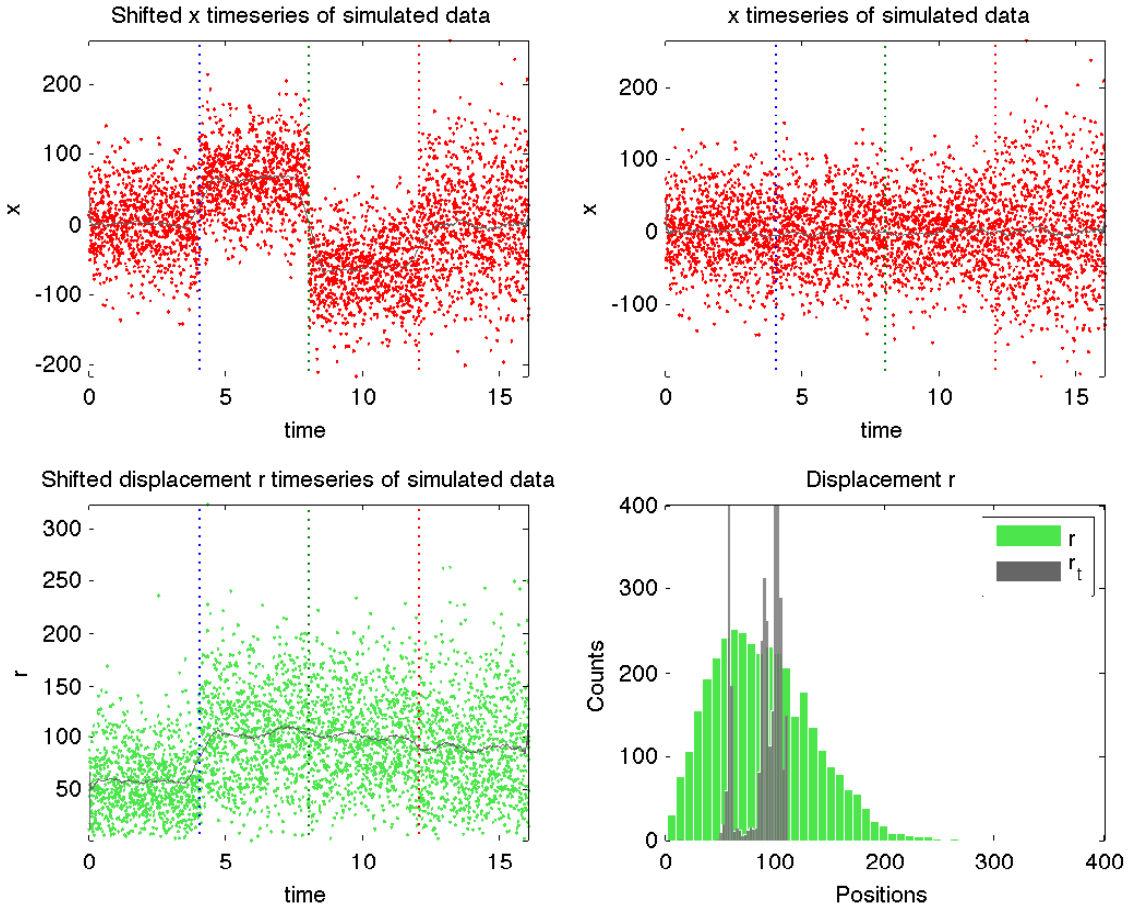

Figure 5.5: Upper left: Wrong normalized x positions with $x|_\tau$. Each movie appears shifted relative to one another. Upper right: Correct normalized x positions with $x|_\tau$. Lower left: Displacement r and $r|_\tau$ assessed from x shown in upper left (and the corresponding y not shown). Lower right: The corresponding histograms for r and $r|_\tau$.

5.3 Quality control

Bead motion symmetry.

It is assumed that a single tethered bead has an isotropic motion around the anchor point. In order to discard beads that are not single tethered a symmetry factor is establish.

In figure 5.6 the anisotropic motion of a bead conducted from a real experiment is shown. The anisotropy is clear from the scatterplot and the positions histograms in this extreme case. From the standard deviations of x and y sampled every second as seen in figure 5.6c the anisotropy clearly stands out. The standard deviations (or variances) can in this case yield a symmetry factor for motion in the x and y directions: $\frac{\sigma_x}{\sigma_y}$. But since the bead motion is random in the (x, y)-plane $\frac{\sigma_x}{\sigma_y}$ cannot always be used as a reliable symmetry factor. Imagine e.g. that the elliptic scatterplot is tilted around the anchor point in a 45° angle. The symmetry factor would then be close to 1 if only the the values of the x- and y-axis are considered. Instead the *principal components* can be used.

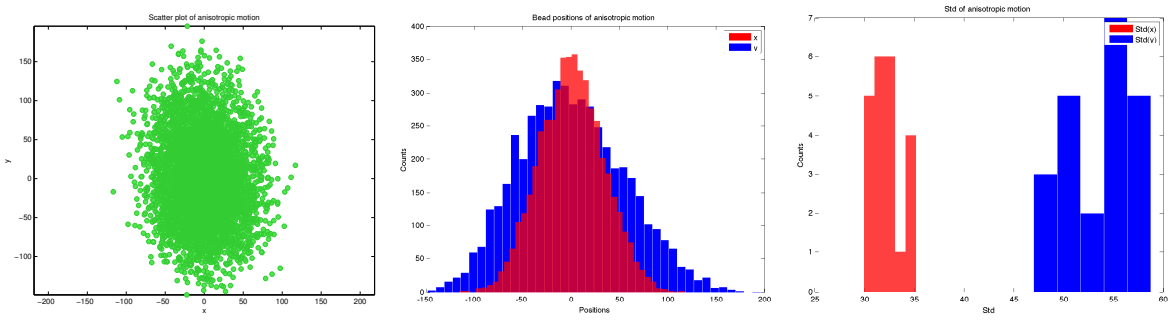

(a) (b) (c)

Figure 5.6: (a) A scatterplot of x and y coordinates for anisotropic bead motion. (b) Histograms of the r and coordinates for anisotropic bead motion. (c) Standard deviations of x and y sampled every 1 second.

The principal components of a dataset can be thought of as containing the variances between variables such that the first principal component comprises the largest variance, and the second component the smallest. The eigenvector with the largest eigenvalue of the covariance matrix is the first principal component of a dataset. The eigenvalues are called the coefficients of principal components. Applied to a dataset x and y is transformed into positions along the principal component. Since eigenvectors are always perpendicular to each other the principal components constitute two new axis which can be used as a measure of symmetry by the ratio of their coefficients:

$$s = \frac{c_{PC2}}{c_{PC1}}, \tag{5.15}$$

where s is the symmetry factor, c_{PC1} the largest principal component coefficient, and c_{PC2} the smallest principal component coefficient [29, 9]. A perfect circular isotropic motion of a bead is expected to have a symmetry factor of $s = 1$.
The covariance can be found between each pair of variables, $(x_{(1)} \ ... \ x_{(n)})$. The x and y comprises two variables in our experiment (so $x_{(1)} = x$ and $x_{(2)} = y$). In general for more dimensions the covariance matrix is defined as

$$cov(x_{(i)}, x_{(j)}) = \overline{x_{(i)}x_{(j)}} - \bar{x}_{(i)}\bar{x}_{(j)} \tag{5.16}$$

which gives the entries of an $n \times n$ matrix with diagonal elements being the variances. From this covariance matrix the eigenvectors and eigenvalues are found. The principal components can then be found from the product of the eigenvector matrix (ordered from the largest to smallest eigenvalue) and the original data matrix.
Beads that are tethered by multiple plasmids often show anisotropic motion as they are restricted more in some directions than others. These appearances can be discarded from the sample collection with the use of the symmetry criterion. The symmetry factor, s, for the anisotropic motion shown in figure 5.6c is $s = 0.36$. The symmetry criterion was set to

$$s \geq 0.8 \tag{5.17}$$

and datasets with $s < 0.8$ were discarded.

Unspecific binding

A bead can bind to the surface without a tether. The polystyrene beads are hydrophobic and the hydrophobic interactions can cause them to agglomerate or stick to the surface even though they are coated in streptavidin proteins. This unspecific binding to the surface still allow for some bead fluctuations. The scatterplot and corresponding histograms for an unspecific bound bead can be seen figure 5.7.
The motion of an unspecific bound bead can be isotropic and therefore get pass the symmetry criterion. The fluctuations are, however, smaller than for a normal tethered bead,

at least for the tether lengths in this experimental study. Since most unspecific binding events are expected to have smaller fluctuations than tethered events a threshold was made to sort these events out. The average displacement, $\langle r \rangle$, was required to be of a minimum length. In general unspecifically bound beads will be omitted by the displacement and the symmetry criterion. The displacement criterion was set to

$$\langle r \rangle_{\min} \geq 60 \text{ nm} \tag{5.18}$$

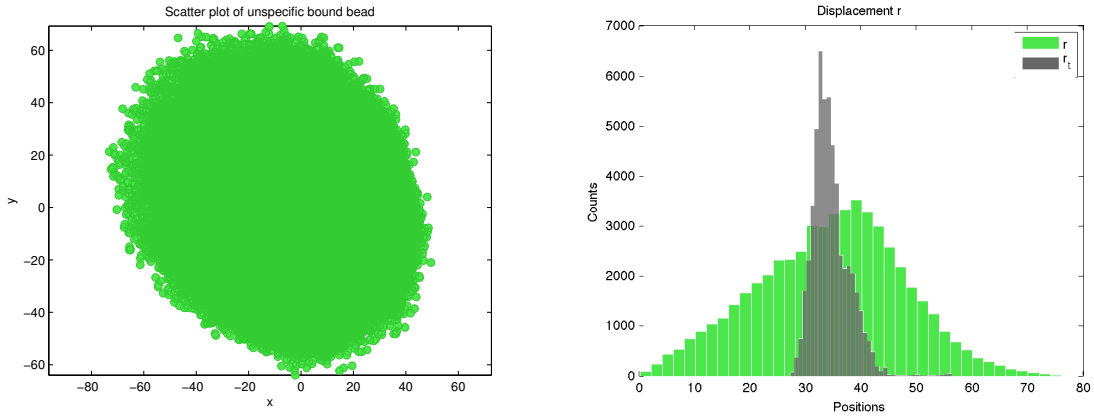

(a) (b)

Figure 5.7: (a) A scatterplot of x and y coordinates for motion of a unspecific bound bead. (b) Histograms of r and $r|_\tau$ for the unspecific bound bead. An unspecific bound bead can show isotropic motion but the displacement r is smaller than for a tethered bead.

Transient sticking events.

During tethered bead motion the bead could transiently stick to the surface. A sticking event can be seen in figure 5.8 between 100–200 seconds. The fixed time trace resembles the fixed bead at the surface. The trace can be fixed at any level on the r scale but has a very characteristic constant amplitude and narrow fluctuation pattern. Sticking events where therefore easily pointed out by visual inspection of time series. If the sticking event was only transient as is the case for the shown time series then the position data in that period was discarded from the dataset. Else the whole experiment was discarded. It was not unusual that the bead permanently stuck to the surface during an experiment.

Apparatus drift and noise.

To visualize any possible drift in the apparatus a bead at the surface was tracked as seen in figure 5.9a. The sample was prepared as a normal TPM sample but without DNA present (step 3 described under *Functionalization of the surface* in section 4.2). As seen from the slope (red line) of -0.008 $^{nm}/_{s}$ there is hardly any drift during the 60 second period. The drift is therefore considered negligible.
Any possible drift could be corrected by subtracting a moving average from the position data. This procedure is exemplified in figure 5.9b where a large drift in the x position trace (red) have been corrected by subtraction of a moving average of 2 seconds (grey).
The contribution of noise in bead movement can be seen from the fluctuations in r. It is a sum of noise induced from the apparatus and the precision with which the bead tracking algorithm positions the bead. It is not possible to distinguish the two contributions from each other in the time series but together they yield a standard deviation of $\sigma_{\langle r \rangle} = 3.7$ nm an amplitude in r below ± 10 nm for the smoothed trace which is considered small compared to a tether extension event discussed in "Results" chapter 6.

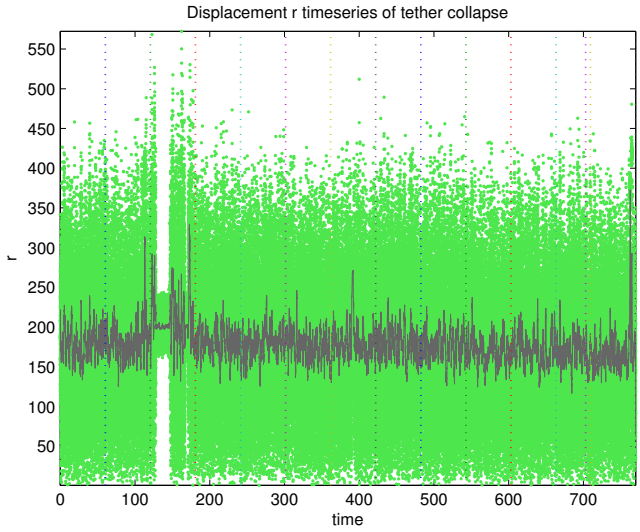

Figure 5.8: Timeseries of displacement r with a tether collapse event between 100-200 seconds. Position data of a collapse is discarded from a data set if it is only transient.

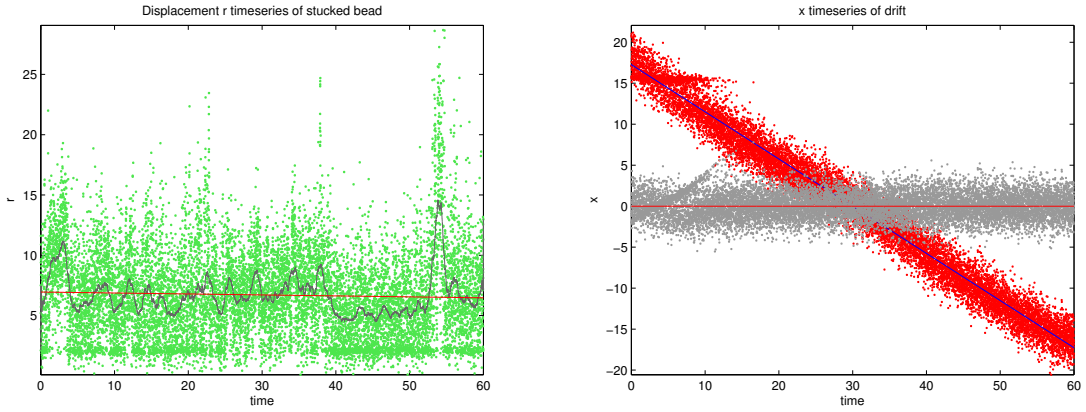

(a) (b)

Figure 5.9: (a) Timeseries of displacement r of a bead at the surface with a linear fit (red line) with slope -0.008 $^{nm}/_{s}$. The standard deviation is $\sigma_{\langle r \rangle} = 3.7$ nm. The sample was wade as normal but without DNA present. (b) An example of drift correction. A position trace (red) with a linear fit (blue) is corrected from drift by subtraction of a moving average to yield the corrected position trace (grey) with a linear fit (red).

Chapter 6

TPM Results

From the simulated data the attention is now turned to the experimental data. Datasets were selected on the basis of the symmetry and minimum displacement criteria mentioned in section 5.3: $s \geq 0.8$ and $\langle r \rangle_{\min} \geq 60$ nm. Approximately 80 % of the datasets that met the criteria showed a symmetry of $s \geq 0.9$.

6.1 Average displacement $\langle r \rangle$

The distribution of the average displacement, $\langle r \rangle$, for 18 tethered beads before topoisomerase was added can be seen in figure 6.1a. The mean value with standard error on the mean is $\mu_{\langle r \rangle} = 157 \pm 13$ nm (indicated by the grey dashed line) and has the standard deviation $\sigma_{\langle r \rangle} = 52$ nm. The impact on $\mu_{\langle r \rangle}$ from the outlying value $\langle r \rangle \simeq 340$ nm is seen when it is omitted (red dashed line) which has $\mu_{\langle r \rangle} = 147 \pm 7$ nm and $\sigma_{\langle r \rangle} = 26$ nm. The value is included in the histogram since it can not be excluded as an artifact. It could be a tether with very few or no supercoils.
The distribution shows that $\langle r \rangle$ is spread around the mean with $\sim 2\sigma$ when the outlier is not included. When it is included the distribution is spread $\sim 3\sigma$ to the right of the mean. The broad distribution of the average displacement seems in accordance with the variation in supercoiling degree mentioned in section 4.1 since this will reflect in $\langle r \rangle$.

Root Mean Square Deviation (RMSD).

In an earlier TPM study by M. Anderson presented in reference [32] the distribution of the $RMSD$ was found for the same plasmid as used in the present study. The $RMSD$ is given by $\sqrt{\sigma_x^2 + \sigma_y^2}$, where σ is the standard deviation given by $\sigma^2 = \frac{1}{n}\sum_{i=1}^{n}(x_i - \bar{x})^2$. The $RMSD$ is different from $\langle r \rangle$ given by $\frac{1}{n}\sum_{i=1}^{n}\sqrt{(x-\bar{x})^2 + (y-\bar{y})^2}_i$. The summation takes place inside the square root when the $RMSD$ is calculated and outside when $\langle r \rangle$ is calculated. The $RMSD$ distribution was also found in low salt concentration by Kamilla

Nørregaard and comparison between these two and the $RMSD$ distribution found in the present study can be seen in table 6.1.

Table 6.1: μ and σ of the $RMSD$ distribution for three different studies on the same plasmid. The study by M. Anderson and the present study are in good agreement while the study with low salt concentration show that ions in solution have a large impact on bead fluctuations as expected.

	μ / σ $_{RMSD,M.\ And.}$ †	μ / σ $_{RMSD,low\ salt}$ ‡	μ / σ $_{RMSD,present}$ ¤
Supercoiled	170 / 76 nm	132 / 40 nm	170 / 59 nm (159 / 30 nm)
Relaxed	255 / 75 nm	143 / 54 nm	–

† From the study of M. Anderson in high salt concentration.
‡ In λ-buffer with low salt concentration of [KCl]=50 mM [32].
¤ From the present study in high salt concentration. Values in parenthesis is without the outlying value $\langle r \rangle \simeq 340$ nm.

The compared mean values under same conditions are in agreement with each other. Outliers were also found in the other studies. The bead used were also of the same size. Therefore the tethers in the present study seems to behave as expected from earlier studies.

The relationship between $\langle r \rangle$ and $RMSD$ is plotted in figure 6.1b. Whether $\langle r \rangle$ or $RMSD$ are largest depends on the variance in the dataset. At some point for larger variance the value of $RMSD$ will exceed $\langle r \rangle$. All vaues of $RMSD$ were larger than $\langle r \rangle$ by a small extend as all points lay below the diagonal in figure 6.1b. The relationship is linear as all point lies in strait line and $\langle r \rangle$ and $RMSD$ can therefore be used as similar quantities for expressing the fluctuations in bead motion.

Low salt concentration.

From the study in low salt concentration shown in table 6.1 it is seen that the ion concentration has an impact on fluctuations of bead motion. The negatively charged backbone of DNA decreases the flexibility due to repulsion along its length. When screened by positive ions the repulsion decreases and the flexibility increases. The flexibility of a polymer is quantified by its persistence length which is the characteristic distance over which the orientation of the chain becomes uncorrelated [39]. The persistence length decreases with an increase in ionic strength. It is therefore expected that a decrease in salt concentration shifts the behavior of the plasmid towards that of a rigid rod. A more rigid plasmid makes smaller fluctuations as indicated by the lower $\mu_{RMSD,low\ salt}$. The rigid rod behavior becomes of importance when distinguishing the plasmid in a supercoiled state from that in a relaxed state under low salt conditions. It was shown that the distribution of relaxed plas-

mids in low salt concentration had a mean of $\mu_{RMSD} = 143$ nm with $\sigma_{RMSD} = 54$ nm [32]. The shift in mean value from the supercoiled state to the realxed state is only ~ 10 nm in low salt concentration. This indicates that it would be difficult to distinguish supercoiled from relaxed plasmids, and thereby topoisomerase activity, in low salt concentrations.
In normal salt concentrations (the concentration used in the present study) the distribution for relaxed plasmids had $\mu_{RMSD} = 255$ nm with $\sigma_{RMSD} = 75$ which gives a shift in mean value from supercoiled to relaxed plasmids of ~ 85 nm. Topoisomerase activity can hence be measured.

Typical dataset.

The study did not show a clear tether extension event as a sign of topoisomerase activity for any of the observed tethered beads. A typical time series and the corresponding histogram of tethered bead motion can be seen in figure 6.2. Topoisomerase was added after approximately 100 seconds. The symmetry was $s = 0.94$. The individual movies are indicated by the vertical lines. The bead tracking algorithm exclude images if the contrast is to low to distinguish the bead from the background. This was not unusual in local periods of a time series. Any periods of excluded images will result in shorter intervals between the vertical lines (but this is not the case in the shown time series in figure 6.2a).

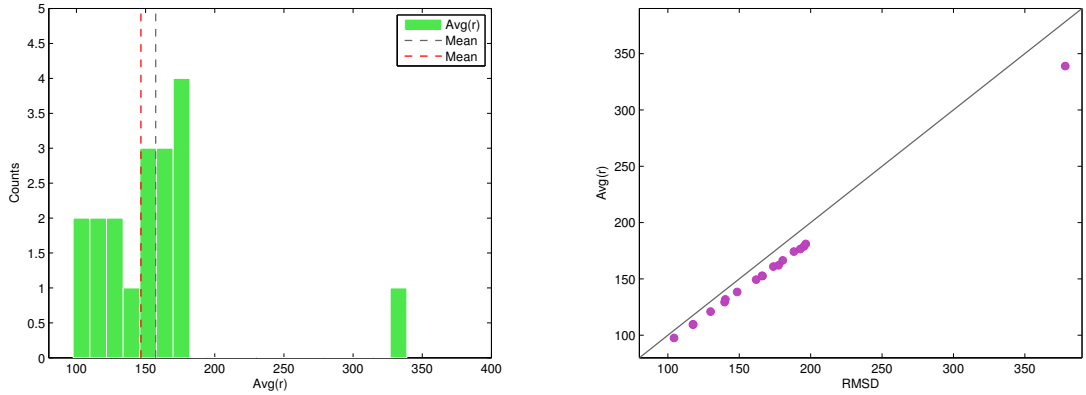

(a) (b)

Figure 6.1: (a) Distribution of $\langle r \rangle$ for tethered beads. The mean value (grey dashed line) is $\mu_{\langle r \rangle} = 157 \pm 13$ nm and has the standard deviation $\sigma_{\langle r \rangle} = 52$ nm. The mean value without the outlying value at ~ 340 nm (red dashed line) is $\mu_{\langle r \rangle} = 147 \pm 7$ and $\sigma_{\langle r \rangle} = 26$ nm. (b) Scatterplot of $\langle r \rangle$ and the RMSD.

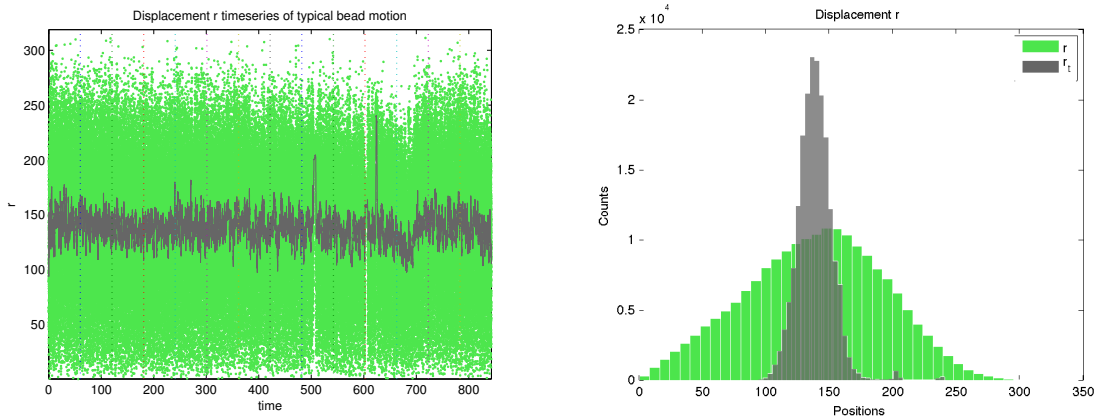

(a) (b)

Figure 6.2: (a) $\langle r \rangle$ and $\langle r \rangle_\tau$ for a typical tethered bead motion showing no extension event. (b) The corresponding histogram of the time series in (a).

6.2 Tether extension event

Only in one experiment could a tether extension event be observed as shown in figure 6.3. The average values of displacement r are indicated with red lines and are from left to right $\langle r \rangle = [98.1, 135.2, 90.3, 124.4]$ nm. The extension event occurs twice. There is a consistency in the extensions as both events show an increase of ~ 35 nm. Prior to the extension event $\langle r \rangle$ lies $\sim 2\sigma$ left of the average mean found in figure 6.1a. The bead motion is therefore close to the lower limit for what has been observed through all experiments. The shift in r is also far from the mean shift of 85 nm between supercoiled and relaxed plasmids as seen in table 6.1. Notice the increase in amplitude of fluctuations for the extension event. This is clearly distinct from a sticking event as shown in figure 5.8. Finally, the shift turned out reversible which is not in accordance with topoisomerase IA's activity as it only relaxes negative supercoils (under normal tension conditions). Whether it is topoisomerase that causes the conformational changes leading to changes in bead motion is therefore not sure.

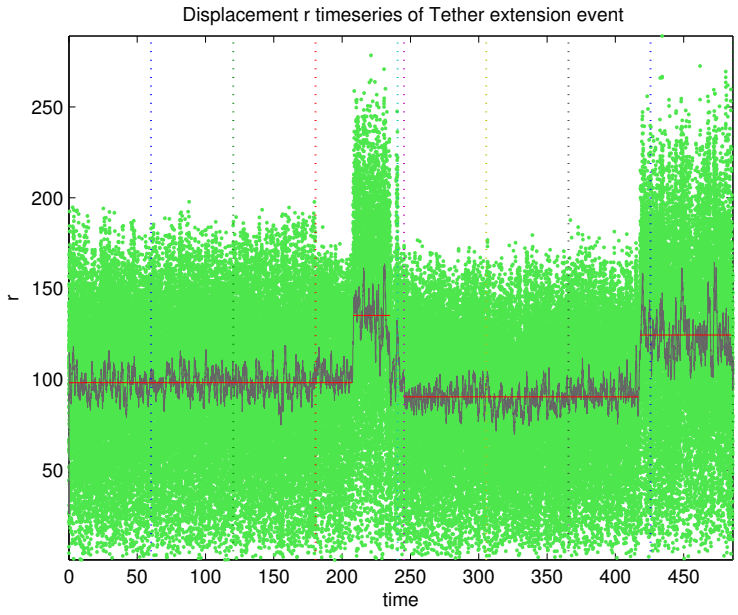

Figure 6.3: Tether extension events. Topoisomerase was added after 100 seconds. The red line indicates average values. They are from left to right: $\langle r \rangle = [98.1, 135.2, 90.3, 124.4]$ nm. The symmetry was $s = 0.83$ before the extension event.

The histograms for the tether extension event is shown in figure 6.4. The left histograms give the displacement r and the smoothed displacement $r|_\tau$. The two different distributions of r are only noticeable from the smoothed values. To get a distinct view of $r|_\tau$ values purely related to the extended states, the $r|_\tau$ values in the time ranges 210–235 and 420-485

seconds are shown in grey in the right histograms. The values in the two time ranges are distributed well within each other.

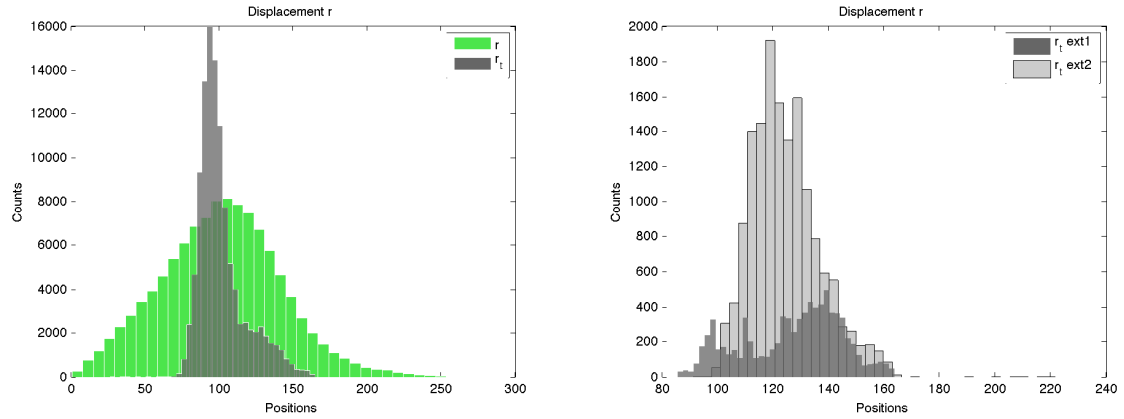

(a) (b)

Figure 6.4: (a) The histograms of r and $r|_\tau$ for the tether showing extension events from figure 6.3. (b) The histogram of r_τ in the time ranges ∼210–235 and 420-485 seconds. The histograms in grey in (b) thereby purely represents r values for the extended tether.

The average displacement r sampled over a period within a dataset, $\langle r \rangle|_\tau$, is shown with the corresponding $RMSD$ sampled over the same period, $RMSD|_\tau$ in figure 6.5. The quantities follow each other for both values of τ which was also indicated by the linear relation in figure 6.1b. However notice how the $RMSD$ values (green) is shifted from being the lowest values to being the highest values as τ goes from 1 second to 8 seconds. The graphs therefore serves to show that both quantities visualize bead motion similar but can vary in absolute values in relation to each other.

Velocity

The velocity of the extension events are estimated as illustrated in figure 6.6. The three figures are zooms of figure 6.3 and the slopes of linear fits to data (in red) give the velocities. They are from left to right $v = [44.1, -2.8, 22]$ $^{nm}/_{s}$.
The ionic strength of the solution inflicts on DNA persistence length. The Mg^{2+} ion concentration specifically inflicts on activity of topoisomerase as the rate is slowed down by a decrease in Mg^{2+} concentration [16]. The velocity is therefore dependent on the ions in solution regardless of whether the extension is caused by topoisomerase or not.
The slopes used to estimate the velocities are based on the moving average smoothed traces. The transition from the prior level to the extended level of r is therefore naturally a sliding transition (a smooth transition). The velocity of the transition is therefore influenced by

the smothering and will decrease with increasing τ (the size of the moving average window). Due to lack of datasets showing tether events statistics cannot be made to yield $\langle v \rangle$ and conclusions cannot be made from the velocities estimated here. Alone the large difference in velocities between the first and second extension event indicates this.

6.3 Gaussian fits

The tethered bead motion is not completely Gaussian distributed as mentioned in section 3.1. This is shown for the experiments conducted here in figure 6.7. The histograms represent x positions (red) and y positions (blue) of a typical tethered bead motion with the corresponding Gaussian fits. The non-Gaussian behavior can arise from the excluded volume effect that leads to an entropic force driving mean position towards a larger value [38]. In a random walk description the excluded volume effect causes the steps of the chain to be dependent of each other near the surface. When the positions are no longer independent the combined effect of the variables will no longer follow the central limit theorem as some variables dominate the distribution. The distribution is therefore not completely Gaussian. This non-Gaussian distribution of bead motion in TPM data is well known in the field and the distributions shown in figure 6.7 serve to show that the experiments conducted in the present study are in accordance with normal TPM experiments.

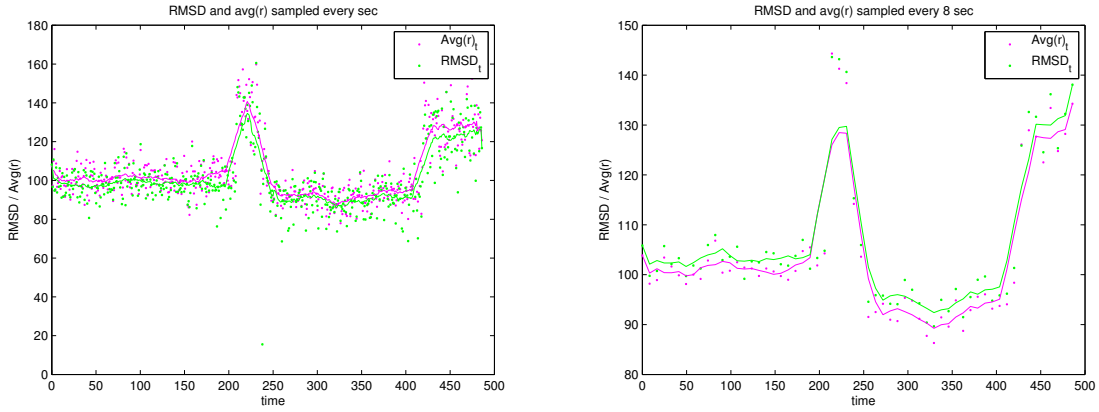

(a) (b)

Figure 6.5: $RMSD$ and $\langle r \rangle$ sampled every (a) 1 second and (b) 8 second for the time series showing a tether extension event in figure 6.3.

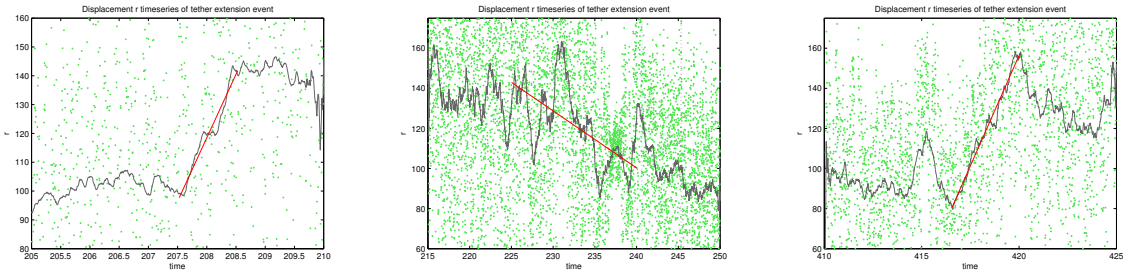

(a) (b) (c)

Figure 6.6: Rates for the reversible tether extension events seen in figure 6.3. (a) $v_1 = 44.1\ ^{nm}/_{s}$, (b) $v_2 = -2.8\ ^{nm}/_{s}$. (c) $v_3 = 22\ ^{nm}/_{s}$

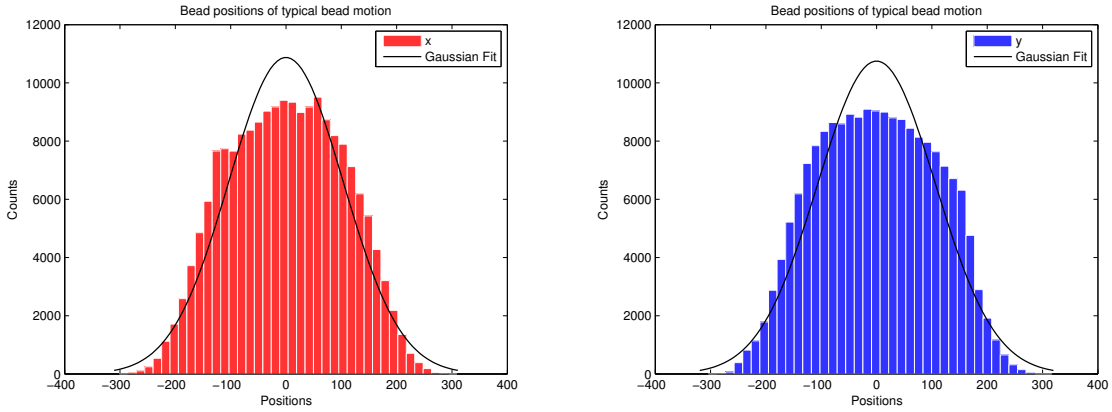

(a) (b)

Figure 6.7: Position data of (a) x coordinates and (b) y coordinates with a Gaussian fit. The bead motion deviates slightly from a Gaussian distribution as expected for restricted brownian motion.

6.4 Discussion

The displacement vector r seemed like a simple and effective choice of visualizing tether extension events as demonstrated with the simulated dataset. A reversible change in tether extension was observed but the lack of reproducibility excluded the possibility of determining whether this behavior was characteristic. The reversibility of the event does not seem to be consistent with the molecular mechanism of topoisomerase IA in that the enzymatic pathway is only known to relax negative supercoils in DNA molecules in native states.

A molecular barrier.

In order for topoisomerase IA to initiate relaxation it must locally unpair the two DNA strands. If the unpaired state is thermodynamically inaccessible for the enzyme it cannot proceed with the relaxation. The equilibrium can be shifted through mechanical stress (e.g., a DNA molecule melts when stretched to a certain level) and hence the degree of supercoiling can form a molecular barrier for topoisomerase activity. Negative supercoiling favor the unpairing of bases in DNA and must be present to a certain degree in order for topoisomerase to pass the barrier. In this project the degree of supercoiling was the naturally occurring distribution from lysed *E. coli* cells. The activity of topoisomerase was confirmed on this plasmid distribution with a gel electrophoresis. The possibility that the plasmids on average have not been negatively supercoiled to a degree that could initiate relaxation by topoisomerase IA is therefore unlikely.
What is not known from the gel electrophoresis is to what extend the degree of supercoiling affect the plasmids tendency to form tethers. Therefore it is uncertain whether the distribution of supercoiling occurring in TPM experiments follows the naturally occurring distribution. The unlucky scenario would be that only plasmids with an insufficient degree of supercoiling to be relaxed by topoisomerase make tethers.

It has been demonstrated that topoisomerase IA can relax positive supercoiled DNA but only in the presence of a local unpaired region [16]. Hence, to initiate the relaxation the DNA must locally still be in the negative supercoiled state. In the study by Dekker et al. the unpaired region was made by designing a sequence of 12 mismatching nucleotides. A similar approach could be applied for the plasmid used in the present study. Plasmids containing a mismatch would be predisposed for topoisomerase action. If tether extension events are still not found for such designed plasmids it would indicate that the problem was caused by something else than the degree of supercoiling. Such a study was beyond the scope of this thesis.

Unknown plasmid conformation.

The plasmid conformation is really not known in details and most probably far from the

idealized schematic drawing seen in figure 4.1. It is therefore difficult to evaluate on the steric hindering of the enzyme caused by, e.g., a very "knotted" conformation. An earlier study with the same plasmid suggests that the conformation should not be a hindering for protein activity [32]. The plasmid was used in protein mediated DNA looping experiments and tether contraction was found after protein addition [32]. Likewise the plasmids could be cut by an endonuclease which makes a single nick in one strand and relaxes the molecule. Plasmids relaxed in this way were also shown to form tethers. The plasmids were cut in ensemble solution and not in a TPM state by the introduction of endonuclease into a flow chamber. Such an experiment could have been a test of a possible steric hindering arising from the conformation of the plasmid. Endonucleases are greatly used throughout the field of biotechnology because of their reliable and precise nicking properties. If a tether extension event does not follow after addition of endonucleases it could be a sign that the plasmid conformation did not allow the tether to extend.

The unknown conformation is a trade-off between the study of native plasmids and the controlled state of supercoiling. From studies involving magnetic tweezers the controlled introduction of supercoils allowed the determination of the relationship between bead motion and supercoils [22]. In this way the authors found that the release of one plectonemic supercoil corresponded to a bead motion of $\sim$ 50 nm in the vertical direction from the surface. It could be interesting to make the same calibration between $\langle r \rangle$ and supercoil relaxation using the native supercoiled form of DNA.

Another possible steric hindering.

There is a steric hinderence that could possibly at the same time allow tether extension / contraction but disallow full relaxation of the supercoiled plasmid. The bead which is attached to the plasmid through a PNA handle is presumably to large to freely rotate around the helical axis of DNA (especially when the plasmid is in a supercoiled state). When topoisomerase cuts a single strand the relaxation of a plectonemic supercoil happens through twists of the helical axis. If the bead is steric hindered in rotating around the helical axis it could block the process of relaxation at a certain point. Such a partly relaxation would reflect in the extension event observed. If the topoisomerase afterwards dissociates, the bead motion could twist the helix in the opposite direction and cancel the relaxation thereby causing the reversible movement observed. After a second binding event the extension is repeated. As seen from figure 6.3 the two extension events are very similar and clearly distinct from the reversible event as also the rates estimated from figure 6.6 indicate. This proposed mechanism is purely hypothetical but could be interesting to test as it allows both the contraction events observed in Kamilla Nørregaards study [32] and disallows a complete relaxation by topoisomerase.

Sample environment.

Proteins often require a certain temperature and ionic environment in order to function. As many other enzymes topoisomerase is known to require Mg^{2+} ions to be active [16]. To create as optimal conditions for enzyme activity as possible the sample environment was similar to earlier studies and the reaction buffer provided from NEB as seen in table 4.1. At the same time a high salt concentration was desirable for a better detection of a tether extension event. Therefore a slightly modified buffer version was used instead. Topoisomerase was shown to be active in both buffers at room temperature through gel electrophoresis. The concentration of topoisomerase also exceeded the level of dissociation ($K_d \sim 200$ pM) as mentioned in section 4.2. Therefore, it was assumed that the sample environment provided conditions for active topoisomerase.

6.5 Conclusion

The study on topoisomerase IA was carried out using TPM and video microscopy in combination with a novel approach of tethering native plasmids with peptide nucleic acid handles. This approach had already been established and tested in another study on protein mediated DNA looping [32]. The bead functioned as a probe for conformational changes in the tethering supercoiled plasmid. Information on plasmid relaxation resulting from topoisomerase action is transferred via changes in bead motion. The motion was quantified from the projected vector of bead positions in the image plane named the displacement r. Before r was calculated a bead tracking algorithm (the St. Andrews Tracker) was used to track bead positions across consequative images recorded at a rate of 225 fps. From r the TPM experiments showed characteristic bead motion and behavior such as sticking events also known from the literature [38, 29]. The average tether displacement was in accordance with earlier characterizations of the plasmid. After addition of topoisomerase an expected tether extension event was only observed in one experiment. The event showed reversible behavior which is not in accordance with the known molecular mechanism of topoisomerase IA. Whether the extension was caused by topoisomerase is not known and lack of reproducibility makes it impossible to define the behavior as characteristic or not. The same is true for the reversible behavior of the event. A mechanism explaning the event involving a steric hindering effect was proposed but is purely hypothetical.
If further experimentation could reveal a characteristic behavior of extension events additional experiments could involve the variation of Mg^{2+} to influence the reaction rate of topoisomerase. Another single molecule study used this approach to reach a temporal resolution allowing them to observe stepwise relaxation of plectonemic supercoils one at a time [16]. Interestingly they also found that the rate of relaxation decreased with a stretching force applied on DNA with a magnetic tweezer. Since the laboratory where the present study was carried out uses optical tweezers setups a future study on the relation between

force and topoisomerase activity is also possible.

Part II

Rdh54's Behavior on DNA

Chapter 7

Rdh54

The protein Plk1-interacting checkpoint helicase (PICH) is necessary for correct sister chromatid segregation [19]. It is believed that PICH monitors tension when it binds catenated DNA threads, called anaphase bridges, spanning two segregating sister chromatids [7]. Michael Lisby and his group have a hypothesis that the yeast protein Rad homolog 54 (Rdh54) is a homolog to human PICH. Information on Rdh54-DNA binding in relation to DNA tension can shed light on the properties of Rdh54 and its role. In the project described here, a setup to study this relation was therefore attempted established inspired from a previous study.

Prior study of Rdh54.

A single molecule study of the translocation on DNA by Rdh54 (also named Tid1), has been carried out earlier [31]. It was found that Tid1/Rdh54 translocates, in an ATP dependent manner, on double stranded DNA in irregular intervals and in both directions with an average travel distance of ∼10.000 base pairs before pausing or dissociating. The study combined optical trapping with fluorescence microscopy. The protein was labeled with an antibody-fluorophore complex and visualized on a bacteriophage λ-DNA tethered to a streptavidin coated bead. With an optical tweezer the bead was trapped inside a multichannel laminar flow chamber and protein translocation was initiated by moving the bead-DNA-protein complex to a buffer containing ATP. A schematic setup can be seen in figure 7.1a. Recorded fluorescence images were stacked in a sequence showing the translocation of the fluorescent protein towards or away from the bead as a function of time. This spatial representation over time is called a kymograph and can be seen in figure 7.1b. The project by Nimonkar et al. serves as an inspiration for this project.

It was also demonstrated that Tid1/Rdh54 could disrupt a three-stranded DNA structure, a D-loop, due to its translocation on DNA [31], see figure 7.2. Gel electrophorisis was used for this study. In the project described in this report, a proposal of how to take the

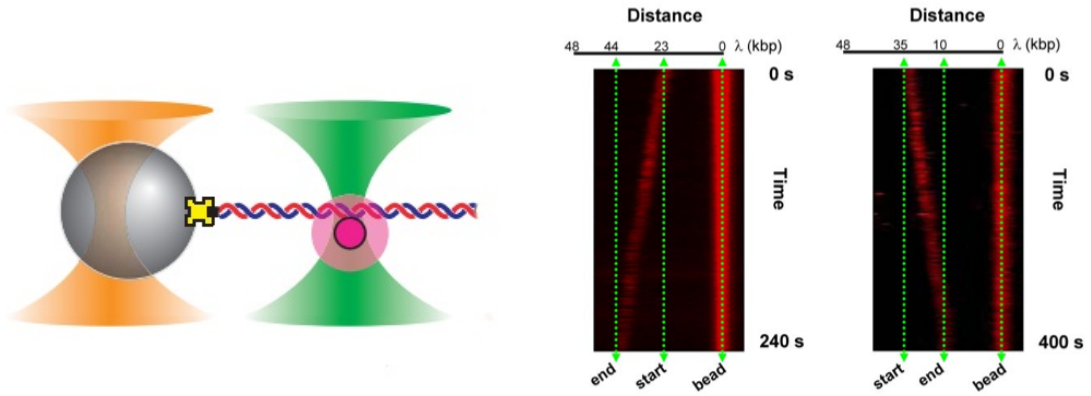

(a) (b)

Figure 7.1: (a) Schematic model of a topical trapped bead-DNA complex with a fluorescently marked protein on the DNA. The trapping laser is shown in orange and the excitation laser is shown in green, and the fluorescence emission is shown in purple. [15]. (b) Two kymographs showing the translocation of fluorescently tagged Rdh54 as a function of time from the the work of Nimonkar et al. [31]. The green lines indicates the start and end position of the protein and the bead position.

disruption study to a single molecule level is made.

Nimonkar et al. do not mention a possible relation between Rdh54 and PICH. In general, literature does not connect PICH's role with Rdh54's and studies on the two proteins characterize them within two distinct cellular systems. Rdh54 is considered being required for mitotic and meiotic recombination and mitotic recombinational repair of double stranded DNA [14, 31] and is not mentioned in relation to resolution of anaphase bridges. PICH is thought to be vital for sister chromatid segregation in mitosis together with Bloom's syndrome protein (BLM) and to be a spindle checkpoint protein although the checkpoint function has been drawn into question [12, 7, 19]. PICH binds to BLM and enables BLM localization to anaphase bridges. PICHs role together with BLM is thought to be of holding anaphase bridges free of histones and thereby prevent nucleosome formation on these bridges before they have been resolved. Both proteins are members of the Snf2 helicase family of chromosome remodeling proteins which are DNA dependent ATPases. Rdh54 is a member of the same family and it would be interesting to test Rdh54's ability to remove obstacles on DNA on a single molecule level.
If a single molecule setup could be established to monitor the translocation of Rdh54 in our lab, we could go on to produce an assay to monitor the disruption of a three-strandet DNA structure on a single molecule level by labeling the third intruding strand with a fluorescence tag. The goals were to: 1) observe localization of Rdh54 on a λ-DNA tether, 2)

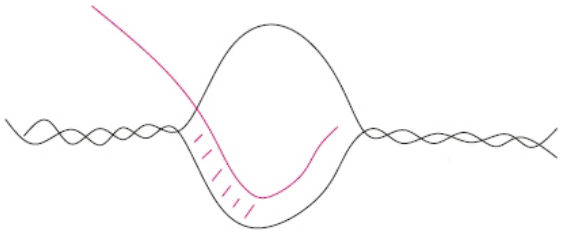

Figure 7.2: Schematic figure of a three-stranded structure called a D-loop. By strand invasion a single stranded DNA invades a double stranded DNA and base pair with a corresponding base sequence. The formation can be made favorable by heating. In cells, proteins like RecA in prokaryotes are involved in strand invasion. If the strand invasion is done with a RNA molecule the structure is called a R-loop.

observe translocation with and without tension in a tethered DNA, and 3) observe disruption of a third strand in a R-loop by Rdh54 translocation on a tethered DNA. In order to study Rdh54 on the single molecule level, TPM and an optical tweezer were combined with fluorescence microscopy. The theoretical background of optical trapping and fluorescence microscopy will be given in the following chapters 8 and 9 but first a brief introduction to the relevant part of the cell cycle related to the biological role of Rdh54 is given.

7.1 Chromosome segregation during mitosis

Cell division is an exquisitely orchestrated mechanism of the cell cycle. It is of vital importance for the cell that the chromosomes are duplicated and segregated properly into the daughter cells. The cell cycle is therefore controlled in every stage through checkpoints. A few main checkpoints divide the cell cycle into phases as seen in figure 7.3a. Following such a checkpoint the chromosomes are duplicated in the synthesis (S) phase. Each duplicated chromosome constitutes two sister chromatids. The cell enters a gab (G2) phase with another checkpoint before the sister chromatids are segregated into individual nuclei in the mitosis (M) phase. Again the cell cycle proceeds after a checkpoint and the cell compartments and cytoplasm are divided into two new daughter cells (cytokinesis).
The mitosis is kicked off by the phosphorylation of a series of proteins which leads to the assembly of the mitotic spindle, see figure 7.3b. The mitotic spindle constitutes the machinery responsible for attaching and pulling sister chromatids to each pole of a cell with the use of microtubules. It attaches to sister chromatids through the kinetochores, see figure 7.4a.

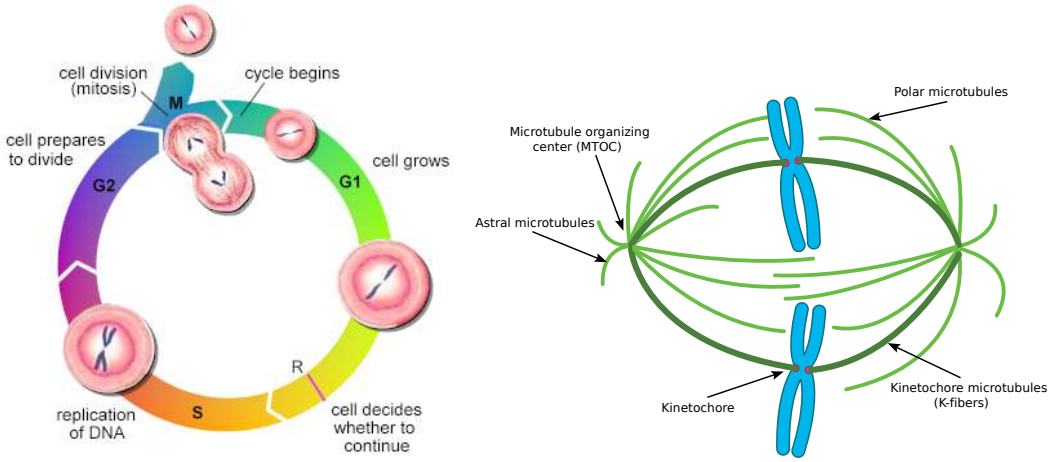

(a) (b)

Figure 7.3: (a) The phases of the cell cycle including the mitosis (M) phase in which sister chromatids segregates. [17]. (b) The mitotic spindle. Through microtubules attached to the kinetochores of sister chromatids the spindle segregates chromosomes [49].

The second major step in mitosis occurs when the protein cohesin is cleaved which initiates the separation of sister chromatids. Cohesin is a protein complex that holds sister chromatids together and can sustain the pulling forces working in the separation of the chromatids as seen in figure 7.4b. Timely cohesion cleavage is therefore of key importance for correct chromatid segregation.
The subphase of mitosis in which segregation takes part is called anaphase and it is initiated by the anaphase promoting complex (APC). When cohesin is cleaved the mitotic spindle can begin to pull the sister chromatids from each other and shortly after, the separation of the spindle poles (the microtubule organizing centers) begins. The separation of sister chromatids is done by the kinetochore microtubules. These microtubules mainly depolymerize and shorten during the process. Antiparallel pairs of polar microtubules polymerize and elongate. These pairs of microtubules are interconnected by the motor protein kinesin. Kinesin pushes the antiparallel pairs of polar microtubules apart which also helps the segregation process. The astral microtubules are flanked by the motor protein dynesin which pull them towards the cell membrane. As phosphorylation initiated the mitosis, dephosphorylation completes it by triggering events which disassemble the mitotic spindle and lead the cell cycle into cytokinesis.

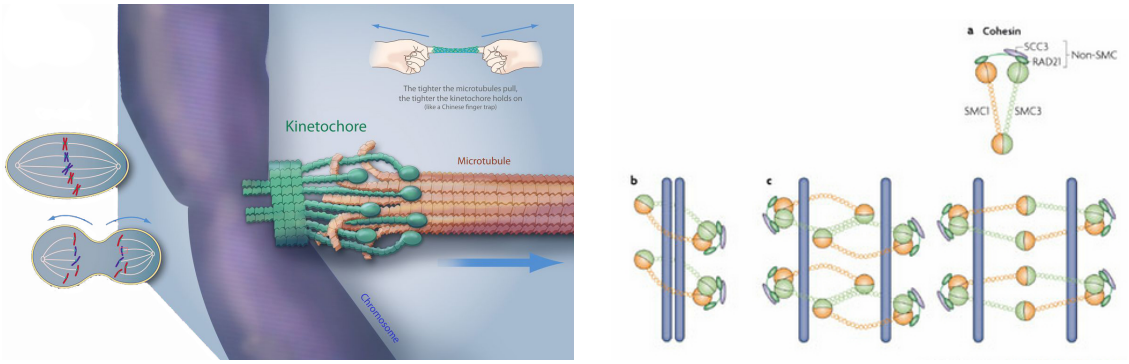

(a) (b)

Figure 7.4: (a). The kinetochore as situated in the center of a sister chromatid [52]. (b) Cohesin holding sister chromatids together. There are different models of the cohesion complex, a, functions. Either one or two complexes embrace the sister chromatids as in b and c [50].

Anaphase bridges.

The chromosomal area where the kinetochores are located is the centromere. It is a region of specialized chromatin that provide the foundation for kinetochore assembly. The kinetochore itself is a protein complex with over 80 different proteins involved in, e.g., microtubule attachment, polymerization and motor protein directed movement and the spindle checkpoint [33].

PICH locates at kinetochores and fine DNA threads connecting sister kinetochores in anaphase; the anaphase bridges [7]. Anaphase bridges constitute chained DNA of sister chromatids, made as a result of DNA replication, and are pulled out from the chromatides when they separate. If the separation of the chromatids begins before the replication process is fully completed an enhanced numbers of anaphase bridges are formed. DNA have a highly dense packed structure at the kinetochores and bridges are especially formed here.

Like PICH, BLM localizes on anaphase bridges [12]. The functions of these proteins in decorating anaphase bridges are not fully understood but a model for how the proteins can facilitate the resolution of these bridges have been proposed [19]. The model propose that PICH-BLM provides a spatio-temporal window in which the cell has time to decatenate anaphase bridges, which otherwise would break and cause micronuclei formation; small nuclei with chromosome fragments separated from the daughter nuclei. Topoisomerase II participates in the decatenation of bridges. In cells where topoisomerase II is inactivated the frequency of PICH positive threads are increased. In cells were PICH and BLM are inactivated the threads are decorated with histones which they are normally not. Histones are protein complexes which wrap DNA and arrange it into chromatin fibers in order to

condense it. The chromatin fibers are the state in which DNA is normally packed inside the eukaryotic cell nucleus. When PICH and BLM are present the threads are not decorated with histones. The model suggests that PICH-BLM prevents the incorporation of histones into the threads and hence allow them to stretch and span long distances without breaking. This should give time for repair enzymes to work and topoisomerase II to resolve the catenated threads.
The mechanistic behavior of PICH in relation to decorating DNA threads have not been studied. Michael and his group have found Rdh54 on anaphase bridges. Therefore we wonder if there can be a relation between the translocation of Rdh54 and its ability of removing obstacles on DNA, and the histone free anaphase bridges necessary for correct sister chromatid segregation.

Chapter 8

Optical Tweezers

Light carries momentum and when photons interact with an object the momentum is transferred to the object. With an intense light source, like a laser, it is hence possible to exert a force in the pico Newton regime, large enough to push or pull objects up to tens of micrometers. This is the principle of optical tweezers. The name refers more precisely to the concept of trapping dielectric objects in a single laser beam which has an intensity gradient and is focused through a lens. The laser beam can be focused through the same lens as used to observe the sample. By such coupling of the optical paths a poweful and yet simple combined tool can be designed to optically trap and control the motion of an object while measuring the force acting on it.

In 1970 A. Ashkin demonstrated the ability of manipulating particles through optical trapping and in 1986 Ashkin and coworkers used a single laser beam focused through a microscope lens to trap a dielectric particle [5]. From this fundamental experimental concept a wide variety of studies especially on biological systems have arisen. Insight in, e.g., molecular motor-protein movement like that of kinesin has been made possible with optical tweezers. Kinesin takes discrete steps along microtubules and is responsible for chromosome movement and vesicle transport[1]. By attaching a dielectric sphere to one kinesin molecule as seen in figure 8 this behavior has been studied [2]. Via the sphere a force can be applied simulating the cargo load and external forces that act on kinesin inside a cellular environment.

The ability to induce and measure forces makes the optical trap a particularly interesting tool for the study of DNA-protein interactions since these often rely on the mechanistic behavior of DNA being a biopolymer. A study also of interest to the project presented in this thesis, looked into the force related disassembly and dissociation of the nucleoprotein Rad51 from DNA [43]. With fluorescence microscopy and kymographs they followed the protein disassembly and found the force dependent behavior of this process. The protein

[1]Several illustrative animations of kinesin stepping have been made and can be found on the web. An example: `http://www.youtube.com/watch?v=4AnPVuzF7CA`

binding was destabilized by ATP hydrolysis and dissociation was helped by DNA tension release.

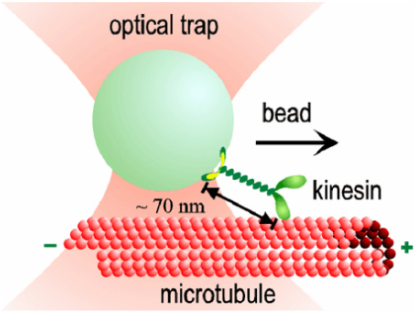

Figure 8.1: By attaching a bead to the motor protein kinesin the molecule can be tracked. With an optical tweezer a loading force can be applied and the impact on its "walking" behavior can be studied. Through this method it was found that kinesin takes 8 nm steps corresponding to the spacing between tubulin dimers which constitute the microtubule kinesin walks along. [23].

The setup used to study binding of Rdh54 on DNA in the present thesis involved an optical tweezer as well. In the following the principles of optical trapping will explained.

Two regimes

When light interacts with an object it is absorbed and scattered (its propagating direction is changed). The momentum transfer due to scattering creates the light forces that is the basis of optical trapping. Scattering is composed of 1) reflection and refraction which depends on the refractive index of the particle, and 2) diffraction which depends on the object geometry. The treatment of these forces can be distinquished by the size of the object compared to the wavelength of the laser light. In general two regimes are considered. The Mie regime in which the diameter of the object is much larger than the wavelength, $d \gg \lambda$, and the Rayleigh regime in which the diameter is much smaller, $d \ll \lambda$. In the Mie regime the light is treated as individual rays and ray optics can be applied. In the Rayleigh regime the object is treated as a point dipole. In the intermediate regime, where $d \sim \lambda$, the finding of the light forces is non-trivial and requires the solution of Maxwell's equations. In spite of this the fundamental understanding of the light forces can be explained by considering a sphere in the Mie regime as in the following section 8.1.

8.1 Ray optics in Mie regime

In this regime the sphere diameter is considerably larger than the wavelength of the incident laser beam: $d \gg \lambda$. The light can be considered as individual rays with discrete momentum, intensity and direction and diffraction effects can be neglected [3].
Consider a laser beam with an intensity gradient decreasing from the center and out, like that of a Gaussian profile as seen in figure 8.2a. A ray will be reflected from the surface and refracted through the sphere volume. The refracted ray is considered in the following. When the photons of the ray are refracted they change momentum (the ray changes direction). In accordance with conservation of momentum the difference in momentum of the incident ray and the leaving ray must equal the momentum transferred to the sphere: $\mathbf{p}_{in} - \mathbf{p}_{out} = \mathbf{p}_{sphere}$. Subtracting the momentum vectors gives us the change in momentum and hence the direction of the resulting force from that particular refracted ray as denoted $\mathbf{F}_a$ and $\mathbf{F}_b$ in figure 8.2. The force magnitude depends on the photon flux and hence on the intensity of the ray which causes $\mathbf{F}_a$ to be larger than $\mathbf{F}_b$. Both these forces have a component along the beam axis which in this case is a scattering force, $\mathbf{F}_{scat}$, and a component on the transverse axis named the gradient force, $\mathbf{F}_{grad}$, as it points in the beam gradient direction. The definition of the scattering and gradient force given here is based on the explanation given by A. Ashkin in [3]. Summing all resulting forces from rays diffracted in the sphere, gives a net force which will move the sphere towards the beam axis in a diagonal movement. When the sphere center is on the beam axis the symmetry will result in the cancellation of gradient forces and only a net scattering force would remain. In order to trap the bead the Gaussian beam needs to be focused through a lens as shown in figure 8.2b. Using the same symmetry argument as before the resulting forces $\mathbf{F}_a$ and $\mathbf{F}_b$ give rise to a gradient force component in the direction toward the focal point.

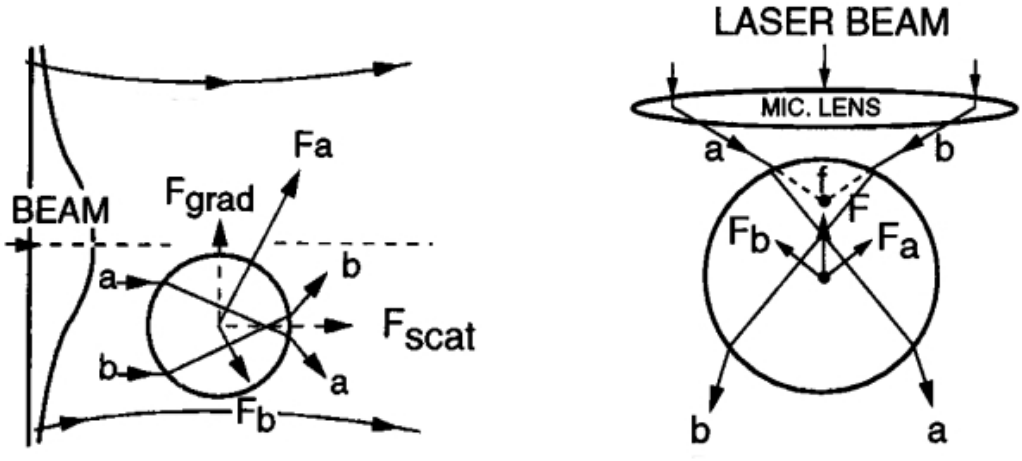

(a) (b)

Figure 8.2: Force diagram in the Mie regime for a sphere in a non-focused (a) Gaussian beam and a focused (b) Gaussian beam. Changes in ray direction gives rise to the resulting forces $\mathbf{F}_a$ and $\mathbf{F}_b$ which have components $\mathbf{F}_{scat}$ and $\mathbf{F}_{grad}$. The single beam must be focused in order to trap the sphere. [4].

The index of refraction is important to consider in this relation. Snell's law is illustrated in figure 8.3a and states:

$$\frac{\sin\theta_i}{\sin\theta_r} = \frac{n_i}{n_r}, \tag{8.1}$$

where θ_i is the angle between the incident ray and the normal to the surface, θ_r is the angle between the refracted ray and the same normal, n_i is the index of refraction of the medium surrounding the incident ray, and n_r is the index of refraction of the medium surrounding the refracted ray. Hence if the refractive index of the sphere is larger than for the surrounding, the ray will be refracted in a smaller angle than the incident angle. This impacts the magnitude of the resulting forces. If the refractive angle becomes larger than the incident, corresponding to a smaller refractive index for the sphere than the surrounding, the net force would point away from the focal point and hence be a scattering force. The reflection of rays from the surface also contributes to the net scattering force and in order to trap a sphere the gradient force must in general exceed the scattering force. Those rays converging most (the rays propagating closest from the lens edge) contribute

most to the trapping force. In order to create a strong trap the numerical lens aperture, NA, must hence be high. The NA is given by $NA = n \cdot \sin\alpha$, where n is the index of refraction of the medium the lens is woking in and α is half the angle that the two marginal rays spans. The larger angle, the larger NA, and the more converging the rays. But since the focal point is given by α (or NA), a high trapping force is of the expense of the trapping depth.
High convergence angles, which is a consequence of a large NA, increase the focus spot size which inflicts on the trapping forces but the perturbations are negligible in the Mie regime.

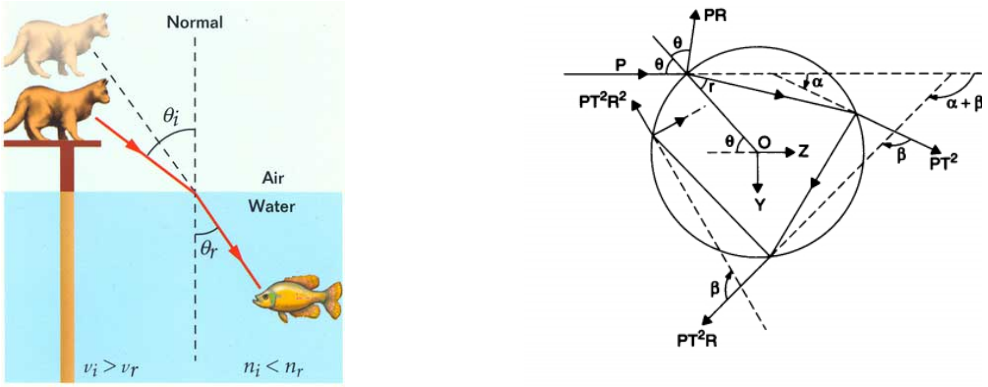

(a) (b)

Figure 8.3: (a) Illustration of Snell's law. The relation between the incident and refracted light angle with the medium index of refraction is shown. (b) An incident light ray of power P will be refracted and reflected over and over in a sphere. R and T are the Fresnel reflection and transmission coefficients [3].

Light forces along the axis.

Incident refracted rays encountering a sphere will be refracted and reflected over and over as shown in figure 8.3b. The ray with power P is reflected and refracted. The first refracted ray is again refracted and reflected and the second reflected ray is refracted and reflected and so on. The total force on the sphere will therefore be a sum of all the contributions from the subsequent refracted rays. The forces F_Z and F_Y along the axis in figure 8.3b can be found with the Fresnel equations using the Fresnel refection coefficients, R, and transmission coefficients, T. It would be beyond the scope of this thesis to go into details about the computation but [3] gives a review and refers to [37] for a detailed analysis. The outcome is a more complete model of the forces acting on the sphere in the Mie regime. So the dominating gradient force component at high converging angles has been

calculated for a polystyrene sphere in water as seen in figure 8.4. The NA was set to 1.25 which corresponds to a converging angle of $\sim$70° and the effective index of refraction was $n = \frac{n_{sphere}}{n_{medium}} = 1.2$. Figure 8.4a gives the magnitude of forces expressed in the dimensionless factor Q from $F = Q\frac{n_1 P}{c}$, where $\frac{n_1 P}{c}$ is the incident momentum per second in a medium of index of refraction n_1 [3]. Q is shown as a function of the distance from the beam focus to the sphere origin on the beam axis where positive values indicate a sphere origin below the focus. The distance is scaled so the radius equals 1. Notice how the gradient force component dominates at all distances away from the equlibrium and the net force, indicated by Q_t, is negative when the sphere origin is above the focus and positive below the focus which means that is always points towards the focus. The equilibrium position, S_E is slightly above 0 (sphere origin) where the weak scattering force component equals the gradient force component. Likewise the gradient, scattering and net force has been calculated as a function of distance on the transverse axis as seen in figure 8.4b. The distance S′ is shown for the left half of the sphere and again given from the origin. From both force diagrams it is seen that the force is linear in relation to the displacement when only small steps of displacement are considered. The optical trap can hence be considered to exert a linear force on a sphere. In the x direction it can be denoted as: $F_{trap} = -\kappa x$, where F_{trap} is the force acting on the sphere, κ is the spring constant, and x is the deviation from the equilibrium position.

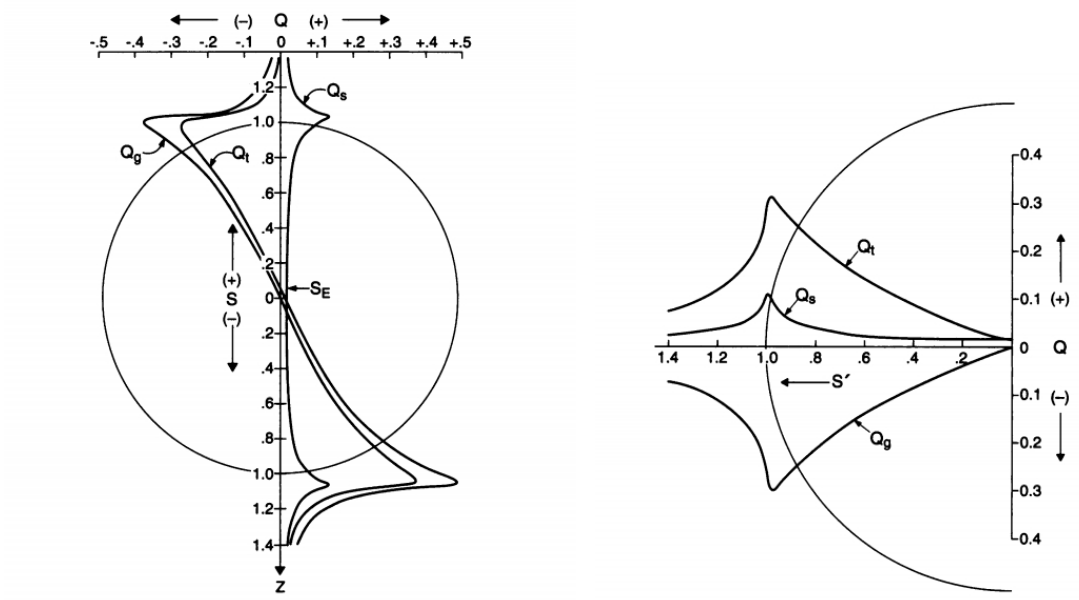

(a) (b)

Figure 8.4: The force components calculated along the beam axis, z, and the perpendicular axis, x, for the displacement of a sphere. Q_g is the gradient force component, Q_s the scattering force component, and Q_t the resulting force component and S is the distance to the origin of the sphere. [3]

.

8.2 Rayleigh regime

If $d \ll \lambda$ objects can be treated as point dipoles when interacting with the light. Again two competing forces are basis for a net force either pushing or pulling the sphere. The scattering of light causes a resultant scattering force along the beam axis dependent on the power, P, of the light scattered: $F_{scat} = n_m \frac{P}{c}$, where n_m is the index of refraction for the medium and c is the speed of light. In terms of the incident photon flux the Poynting vector $\mathbf{S}$ can be used:

$$\mathbf{F}_{scat} = n_m \frac{\sigma \langle \mathbf{S} \rangle}{c}, \tag{8.2}$$

where σ is the scattering cross section which for a sphere is

$$\sigma_{sphere} = \frac{8}{3}\pi(kr)^4 r^2 \Big(\frac{n^2-1}{n^2+2}\Big)^2, \tag{8.3}$$

where k is the wave number $\frac{2\pi n_m}{\lambda}$ dependent on the wavelength λ, r is the object radius, and n is the effective index of refraction.

The propagating electromagnetic field of light induces a dipole moment, $\mathbf{p}$, in the dielectric object given by $\mathbf{p} = \alpha\mathbf{E}$, where α is the polarizability and $\mathbf{E}$ is the electric field. The field exerts a force on the dipole and because of the intensity gradient of the beam the resulting force points along the gradient. This is the gradient force:

$$\mathbf{F}_{grad} = (\mathbf{p} \cdot \nabla)\mathbf{E}, \tag{8.4}$$

where ∇ is the gradient operator working on the electric field. F_{grad} can then be expressed as

$$\mathbf{F}_{grad} = \alpha\nabla\langle E^2\rangle, \tag{8.5}$$

where α is the polarizability of the sphere and $\langle E^2\rangle$ is mean square of the electric field. α depends on the refractive index as $\frac{n^2-1}{n^2+2}$. As in the Mie regime, the requirement that $n_{spere} > n_{medium}$ applies for the Rayleigh regime which keep the fraction positive and thereby $\mathbf{F}_{grad}$ positive. Conversely the force would pushing the sphere away.

8.3 Measurements with optical tweezers

As in the Mie regime the force can be considered linear for small displacements also for spheres with $d \sim \lambda$. To find the force on a sphere in an experiment this realization is used in a calibration procedure.

Force calibration.

To find relation between force and displacement the spring constant κ must be found. By applying a drag force on the trapped sphere κ can be deduced from the correlation of the forces (a calibration). Consider a sphere moving in the x-direction in the optical

trap. The trap exerts the force $F_{trap} = -\kappa x$ as mentioned above. If a drag on the sphere is applied as well, the drag force in the x-direction will be $F_{drag} = -3\pi\eta dv$, where η is the viscosity, d is the diameter of the sphere, and v is the velocity. At constant velocity an equilibrium position exists and by equaling the forces the trap stiffness can be found [34]:

$$F_{trap} = F_{drag} \;\Rightarrow\; \kappa = \frac{3\pi\eta dv}{x}, \tag{8.6}$$

where x is the new position. This is the Stokes calibration since the drag force used is known as Stokes law.
An object moving in a medium can cause turbulence. In order to apply Stokes' law this turbulence must be negligible and a laminar flow should exist. The flow can be characterized by Reynolds number, Re, which is a quantification of the fluids resistance to change in motion and given by $Re = \frac{\rho v d}{\eta}$, where ρ is the density of the fluid and d the diameter of the sphere. To avoid turbulence $Re < 1$. The best experimental conditions to perform the Stoke calibration is far away from the surface since the turbulence arises at higher viscous drag close to the surface.

Chapter 9

Fluorescence Microscopy

In a standard fluorescence microscopy setup, named epifluorescence microscopy, the sample is illuminated with light passing through the microscope lens. Emitted light from the sample is collected back through the lens and detected at the back focus plane. Illuminating light is confined to the excitation wave length spectrum by letting it pass through an excitation filter. With a dichroic mirror the light is coupled into the light path of the lens. The emitted light has a lower wave length spectrum and passes through the same dichroic mirror and an emission filter before it is collected. The dichroic mirror and emission filter ensure that only light in the emission spectrum is collected. Because the sample is illuminated in the opposite direction of which the emission signal is collected the transmitted light will not disturb the image signal and the noise is kept low. The principle of fluorescence microscopy relies hence on the separation between the emitted and much weaker illuminating light signal which differs in wave lengths due to Stokes shift.

One way to improve the resolution of a microscope is with a confocal pinhole. The pinhole allow only light from the focal plane and reduce blurring and enhance contrast.

Confocal microscopy

The advantage of confocal microscopy over standard microscopy is the enhanced resolution achieved by blocking out-of-focus light which else causes blurring. The principal is sketched in figure 9.1a. Using a laser a small sample area can be illuminated at each time step by scanning the laser across the sample surface. The excitation laser (shown in green) illuminates fluorephores which emit light (shown in red). A pinhole is placed in the emission path which only allows the detection of light from the focus plane. The advantages are an increased resolution and the ability to stack image planes and hence create a 3D image. The draw backs is the decreased signal intensity which must be compensated by a longer exposure time. This calls for effective fluorophores with high quantum yields. The point illumination requires laser scanning to image an area. This enhances the recording time of

the image as the scanning rate is limited by the movement of mirrors directing the laser onto the surface.

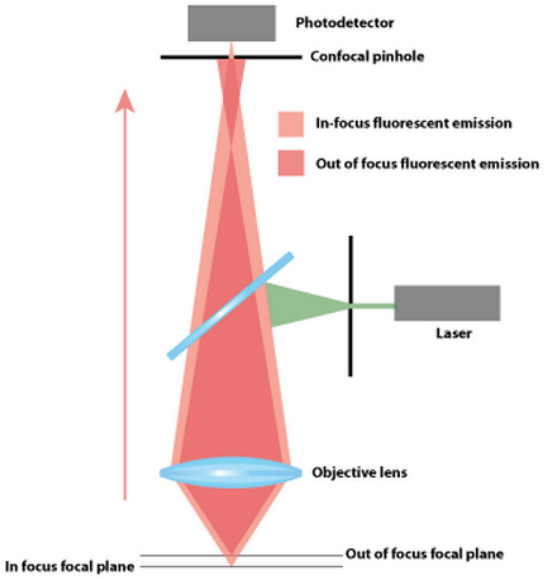

Figure 9.1: Schematic of a confocal microscope. The confocal pinhole blocks the out-of-focus light and image blurring is minimized.

Fluorescence

Fluorescence is the emission of light from a substance which has absorbed electromagnetic radiation. The phenomenon arises when an electron in the ground state absorbes the right amount of energy, $E = h\nu$, to go to an excited state. h is Planck's constant and ν the frequency of light. From the excited electronic state the electron decays through the vibrational states in non-radiative steps to the lowest vibrational excited energy level. From this level the electron decays in one step to the ground electronic state by the emission of a photon. The non-radiative decay causes a loss of energy in the emitted photon which hence has a longer wave length. This phenomena is named Stokes shift.
As mentioned earlier good fluorophores are needed for good resolution because there is a trade-off between signal strength and enhanced resolution. The efficiency of a fluorescence process is given by the quantum yield, Θ, quantified from number of photons:

$$\Theta = \frac{\text{no. of photons emitted}}{\text{no. of photons absorbed}}. \tag{9.1}$$

An efficient fluorophore with $\Theta \sim 0.9$ is Alexa-488 used in this experiment.

Position determination of fluorophores.

The diffraction limit of the point spread function (PSF) for an object observed in an optical system sets the resolution limit. Features smaller than the diffraction limit cannot be directly distinguished. The limit is approximated to be $\sim$ half the wavelength of light: $\lambda/2NA$, where NA is the numerical aperture of the lens. To break the limit and enhance resolution and determine, e.g, fluorophore positions with a greater precision the centers of the PSF's must be determined as they indicate the center positions of the fluorophores. As described in the topoisomerase project a tracking algorithm can be used to find particle positions of consecutive images. When the particles have diameters of sub-wavelengths it has been found that an algorithm based on the Gaussian fit to the intensity distribution performs best [13]. The PSF is well described by a Gaussian function and therefore the intensity profile of pixels in the sub-wavelength level is well approximated by this algorithm. The general two-dimensional Gaussian function is given by

$$G(x, y) = A \exp\Big(- \frac{(x)^2 + (y)^2}{2\sigma} \Big), \tag{9.2}$$

where the Gaussian function is considered centered at origin of the PSF and A are a constant [51]. The parameter σ should be found so that the function best fit the PSF.

Concentration of fluorophores.

Even though the precision of fluorophore position can be determined below the diffraction limit from fitting a function to the PSF, the PSF must still represent only one fluorophore to observe single fluorophores. If two fluorophores are in close proximity their PSF will appear as one. This means that not more than one fluorophore should be present per diffraction limited volume which can be controlled by its concentration which have a maximum limit of $\sim$ 10 nM [44]. If a higher concentration of labeled protein is needed ,e.g., to reach a DNA-protein binding constant higher than this limit, the solution is often to only label a fraction of the proteins and thereby still maintain a high concentration of protein.

Chapter 10

Experiments

Proposals for the experimental setup and quantification of the planed experiments will be presented in the following. The experimental goals were to observe: 1) Rdh54 localized on λ-DNA, 2) Rdh54 translocation on λ-DNA, and 3) disruption of an R-loop by Rdh54 translocation.

10.1 Experimental system

Bioassay.

A TPM bioassay similar to the one used in the topoisomerase project was established. A 16 μm linear λ-DNA molecule was used as tether with a digoxigenin and biotin handle. It tethered a streptavidin coated bead to the surface of a flow chamber coated by anti-digoxigenin. The sample preparation was identical to the one described in step 1,2 and 4 in section 4.2. In step 3 the λ-DNA was added in a concentration of $\sim$ 2 pM.
The essential part of the bioassay is the DNA construct tethering the bead to the surface. Unfortunately it was exactly this part that troubled us and we were unable to observe tethers for a long period. Therefore a lot of time was spend on testing the possible implications preventing tether formation.
The DNA concentration was increased to exclude the possibility that to few observable molecules were present to form bonds between beads and anti-digoxigenin during incubation time. From the procedure of functionalizing the DNA construct with handles, the concentration should be approximately known but the construct was purified by micro spin columns and we could not be sure to which extent the concentration had been reduced. Absorbance measurements could have revealed the concentration but it was uncertain how the handles would inflict on the absorbance. Instead we used the bioassay procedure with enhanced concentrations.
Different biotin coated beads were tried and anti-digoxigenin was exchanged. The protein

coated beads can usually be preserved for a long period but they were on the other hand not brand new. The same was true for anti-digoxigenin. Through control experiments using different beads and anti-digoxigenin that were functional in Kamilla Nørregaards experiments, the possibility that these factors prevented tether formation was excluded.
The attention was then turned to the buffer. The ionic strength is known to impact DNA conformation and different bead behavior had been observed by buffer exchange. E.g. beads tended to collapse to the surface in many samples. Could it be the buffer composition that prevented tether formation or was responsible for collapsing every possible tether before they could be observed? The litmus test was to make samples with the plasmid from Kamilla Nørregaards study as shown in table 10.1. No tethers were found in the buffer used so far (buf_{ori}) and it could be concluded that the buffer had a negative impact on tether formation. The test also showed that the λ-DNA construct did not form tethers to the same extend as the plasmid when tested in Kamilla Nørregaards buffer. The test thus left us with two problems: Neither the DNA construct nor the buffer were optimized for tether formation.

	buf_{Kam}	buf_{ori}
plasmid	tethers	–
λ-DNA	tether/sample < 1	–

Table 10.1: The litmus test. Only in Kamilla's buffer (buf_{Kam}) could tethers regularly be observed.

Both buffers from the litmus test were λ-buffers (mixed as shown in appendix A). The critical difference turned out to be a purification treatment in which Kamilla's buffer had been filtered through a Ficoll gel filter making it very clean. In the purified buffer the number of beads collapsing onto the surface was reduced to a large extend. From here on new stocks of DNA constructs were made and tested but every time with the outcome of very few tethers (tether/sample < 1).[1] The problem had been narrowed down to the DNA construct.

Functionalization of λ-DNA.

The linear double stranded λ-DNA (isolated from the bacteriophage lambda, NEB) has 12 bases of single stranded overhangs in each end:

5'GGGCGGCGACCT3'–λ–3'CCCGCCGCTGGA5'

Notice that the overhangs are complementary. Each overhang are labeled with biotin and digoxigenin to make handles which enables the tethering of a coated bead to a coated

[1] From this point it was decided to move on to another study that led to the project described in the first part of this thesis.

surface. The handles can be prepared by adding single deoxynucleotide tryphospahtes (d-XTP where X is either A,T,C or G) and DNA polymerase. By using a labeled d-TDP, e.g. d-TDP-biotin, the handles are attached to the complementary bases, A, when new strands are synthesized by DNA polymerase on the overhangs. Pre-made handles with digoxigenin and biotin already incorporated in complementary sequences called oligomers are commercially available. Such biotin and digoxigenin oligomers were used in this study and mixed in excess (3:1) with λ-DNA and incubated with DNA ligase at room temperature for minimum 12 hours. What turned out to be important was that the oligomers, complementary to the overhangs and hence to each other, preferred to anneal to each other rather than the λ-DNA overhangs. Therefore the preparation did not yield an amount of functionalized constructs large enough to be observed as tethers in the TPM samples. Adding the oligomers in individual steps changed this and finally tethers could be created and observed in the purified buffer.
A note to add on the DNA construct is that over a period of a couple of months the number of tethers reduced gradually and finally ceased using the normal sample preparation procedure. When this old stock of DNA construct was heated to 60 °C in 10 minutes and cooled down again and used as normal, tethers could again be observed but not in the same amount as from a freshly made stock.

Protein.

Rdh54 was pre-engineered with a polyhistidine-tag and could thereby be labeled with a histidine probe which in this case was a histidine-antibody bound to an Alexa-488 fluorophore (His-probe 15 Alexa Fluor®488, Santa Cruz Biotechnology). Rdh54 and the his-probe were mixed 1:6 to get all proteins labeled. The labeling was performed in the buffer MB seen in figure table 4.1 as the constituents and concentrations were similar to those used in other studies of Rdh54 [31, 36]. The labeled protein was diluted in the range from 0.1 μM to 10 nM through the experiments of localizing Rdh54 on DNA. The protein and his-probe were incubated in 15 min at room temperature and the labeled protein was incubated for another 15 minutes in the flow chamber before observation. After localization of proteins $\sim$ 1 mM ATP should be added to start translocation [31].

R-loop.

The DNA construct for studying Rdh54's ability to remove obstacles from DNA is based on a RNA-DNA hybrid as sketched in figure 7.2. This R-loop can be assembled by annealing DNA and a presynthesized RNA molecule [24]. In the presence of a mild acting denaturant (e.g., formamide) RNA will form a heteroduplex with the DNA template strand through base pairing. The second DNA strand further stabilizes the three-strandet structure as indicated by the very high temperature tolerance of $\sim$ 95 °C reported [24]. By fluorescently tagging the RNA molecule the possible disruption of the R-loop by Rdh54 can be followed.

The position and frequency of R-loops can be controlled by sequence analogy with the RNA molecule along the λ-DNA.

Pump system.

Studies on Rdh54 and Rad51 mentioned in the previous chapters 7 and 8 made use of an elaborate multichannel laminar flow system [31, 43] as illustrated in figure 10.1. By introducing separated parallel buffers, laminar flows could be maintained. Such a system provides a gently and very rapid change of buffer environment when the construct is moved across the laminar flow barrier. Furthermore the flow ensures that excess proteins and fluorophores not specifically bound to DNA is not present in the observed sample volume. In this way the background noise is reduced. The incorporation of a multichannel laminar flow system in the setup was beyond the scope of this study but a simplified single channel system was made with a pump (Pump 11 PicoPlus, Harward Apparatus). An input and output channel was made in a glass slide with a diamond drill. The glass must be of adequate thickness to prevent it from cracking when drilled and water should surround the drill at all times. The glass slide is used to assemble the flow chamber as described in section 4.1. In addition two plastic tubings was fixed to the holes with epoxy. Buffer was introduced through one tube and lead out by the other tube. The buffer are kept in a syringe mounted on the pump. With the pressure driven pump a steady flow can be maintained down to 1.3 pl/min as stated by the provider. In practice the steady flow is heavily influence of the tubings and to maintain a steady flow at low flow rates the buffer should be sucked out at same rate as it is introduced. The pump was not build for making a circulating flow and from the nl/s range is was not possible to maintain a steady flow in the chamber. Instead the flow came in bursts.

Optical tweezers setups

An alternative bioassay was tested in the early stages of the project involving a dual optical trap named the NanoTracker (JPK Instruments). The idea was to stretch a DNA molecule tethering two beads trapped in each beam and through fluorescence microscopy observe Rdh54 on DNA. The tether should be formed by trapping a streptavidin coated bead attached to a DNA molecule and with the other beam trap an anti-digoxigenin coated bead, moving it in close proximity to the first trapped bead and thereby establish a tether forming a "dumbbell" construct. The other strategy was to incubate the different types of beads with DNA and trap the already formed dumbbells. The assay was discarded as it took place at a stage in the project where tether formation was unsuccessful. Furthermore it turned out that the the two beams in the NanoTracker cross-talked leading to a release of a trapped bead in the first trap when the second trap was turned on to trap the second bead. Instead a confocal setup (Leica TCS SP5) with a build-in single optical trap was used and the dumbbell assay was replaced with the TPM bioassay when we managed to

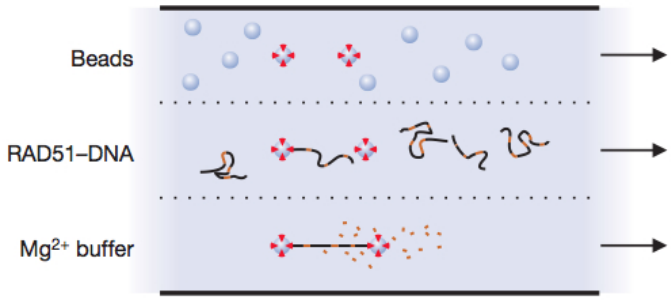

Figure 10.1: Illustration of a multichannel laminar flow system used in the study of the protein Rad51 [43]. With dual optical tweezers it was possible rapid to change buffer by moving two beads tethered by DNA across the laminar flow.

create tethers of λ-DNA.
It was possible to optically trap tethered beads and positioning the DNA nearly horizontally along the surface and to stretch the DNA. After addition of Alexa-488 tagged Rdh54 proteins fluorescence was visible but not as signals from proteins situated on DNA. Instead the fluorescence was located at bead positions. The tagged proteins or the pure fluorophores must therefore cover the beads which is not unexpected from other experiments where proteins are observed to both cover stretched DNA molecules and beads [31]. Unfortunately it was not possible to detect Rdh54 localization on DNA. Whether the protein and fluorophore actually binds to each other was not tested in the present study. We relied on the protein's pre-engineered polyhistidine-tag would effectively bind the fluorophore (an antibody histidine probe).

10.2 Quantifications

A localization of Rhd54 on DNA was not observed in the few experiments carried out so far. Therefore the following is a proposal on how I envision future data could be quantified. An often used visualization of fluorescently tagged proteins translocating on DNA is kymographs: intensity traces made from cutting out the region of interest (ROI) of single frames and concatenate them to build a time trace [31, 43, 36]. The ROI is this case would be the part of an image where the DNA molecule is located. Through a particle tracking algorithm the positions can be determined to sub-pixel precision. Such kymographs were shown in figure 7.1b. Rates for translocation can be quantified from these time traces as the slopes of the intensity time traces. The intensity trace as a function of time can be measured for varying environments such as different ATP concentration or varying tension in the DNA molecule. The translocation (or possible dissociation) rate as a function of

DNA tension could be interesting to quantify especially in relation to Rdh54's possible role of keeping anaphase bridges clear of histones. The rate as a function of tension could be fitted and the relation could yield a characteristic dependence. In a study of RAD51 proteins the disassembly rate as a function of tension in DNA was fitted to yield a dependence described by the Arrhenius' relation $k(F) = k(0)\exp(-xF/k_BT)$ where k is the rate constant, F the force and x the reaction coordinate [43]. It could be equally interesting to find a relation between the possible disruption of R-loops with tension.

10.3 Conclusion

The three original experimental goals could not be reached within the time limit of this thesis. Because of the difficulties related to tether formation there is still a long way to go before the final experiments can be carried out. A possible continuation of the project would be interesting because results could yield new insights of Rdh54's mechanistic behavior and biological role. The establishment of a test-construct involving the R-loop would be interesting to many other studies on mechanistic behavior of proteins. To apply such a construct in a single molecule setup would be an achievement for the laboratory and open many possibilities for future studies.
The experimental work of localizing Rdh54 on DNA is where this study ended. Since other studies on the same protein have managed exactly this, the goal seems within reach by further experimental work with the same bioassay already established [31, 36].

Appendix A

Experimental

A.1 Buffers

All buffers were filtered through a Ficoll gel filter from GE Healthcare.

PEN
10 mM PIPES pH 6.5
0.1mM EDTA
10 mM NaCl

PBS
20 mM Na_2HPO_4
150 mM NaCl
and to store the beads
2 mg/ml α-Casein

λ-buffer
10 mM Tris-HCl pH 7.4
200 mM KCl
0.1 mM EDTA
and to make the washing buffer
2 mM DTT

NEB Reaction buffer
20 mM Tris-acetate
50 mM K-acetate
10 mM Mg-acetate
1 mM DTT

100 mg/μl BSA

Appendix B

Results

B.1 Gel electrophoresis

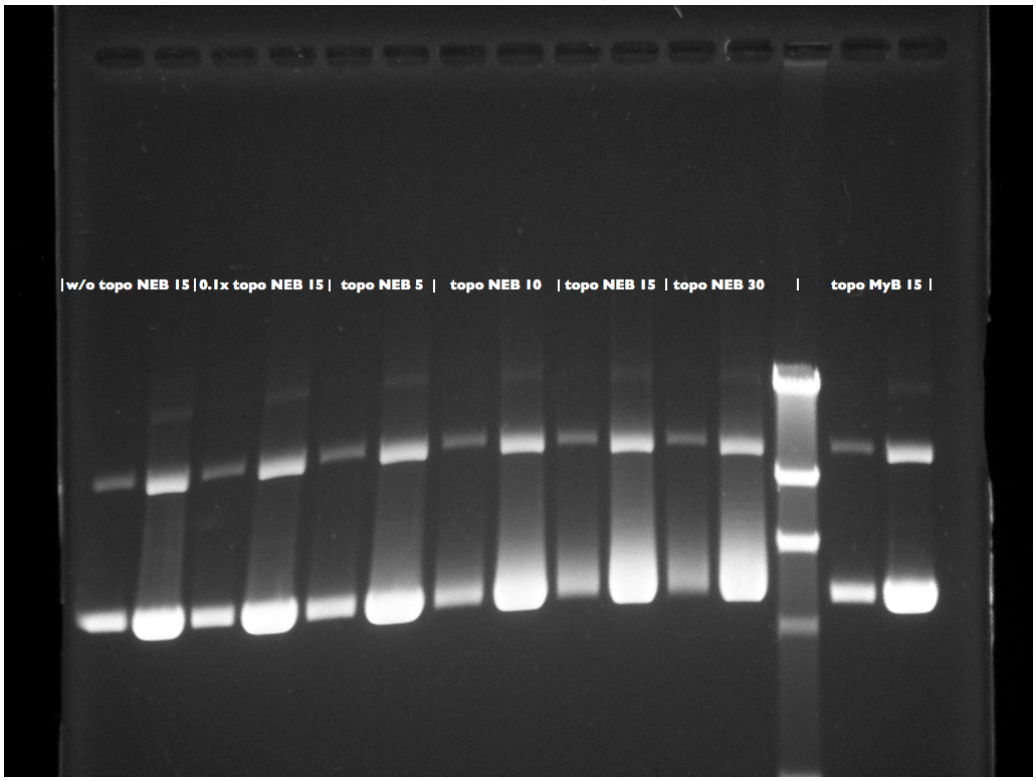

Figure B.1: The stained agarose gel for topoisomerase activity.

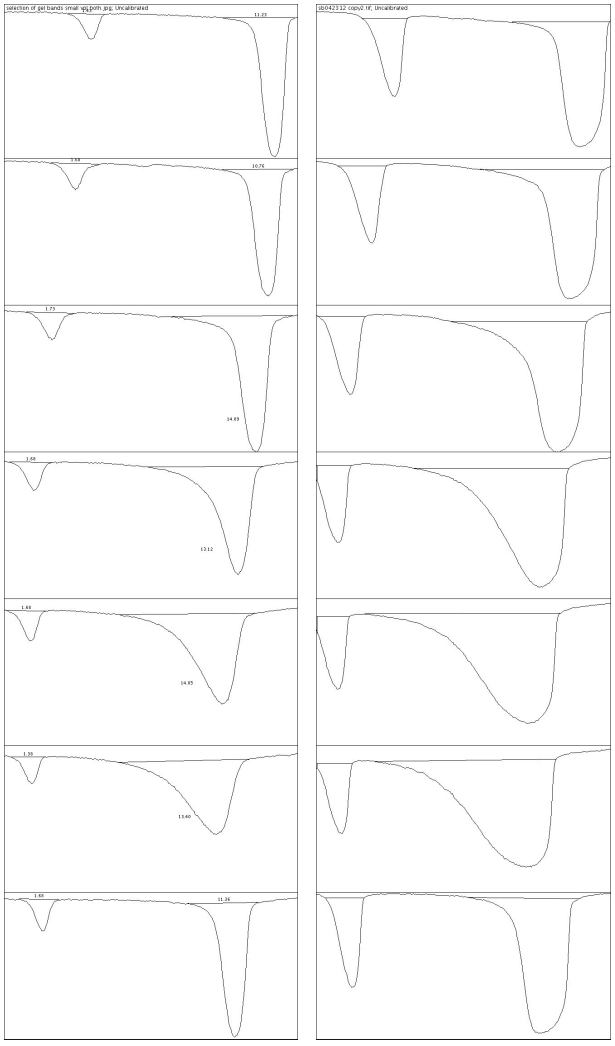

(a) (b)

Figure B.2: The intensity profiles for the (a) 2 μl and (b) 10 μl lanes.

$sample_{2\mu l}$	band	% area	$r_{w/o\ topo}$	% $area_l$	$r_{l\ w/o\ topo}$	$r_{fin/ini}$
w/o $topo_{15}$	ini	1.418	1			7.86
w/o $topo_{15}$	fin	11.231	1	12.7	1	
0.1x $topo_{15}$	ini	1.604	1.12			6.71
0.1x $topo_{15}$	fin	10.761	0.96	12.4	0.98	
NEB_5	ini	1.733	1.21			8.13
NEB_5	fin	14.085	1.25	15.8	1.25	
NEB_{10}	ini	1.683	1.18			7.80
NEB_{10}	fin	13.123	1.17	14.8	1.17	
NEB_{15}	ini	1.679	1.18			8.84
NEB_{15}	fin	14.848	1.32	16.5	1.31	
NEB_{30}	ini	1.383	0.97			9.69
NEB_{30}	fin	13.398	1.19	14.8	1.17	
MB_{15}	ini	1.682	1.18			6.76
MB_{15}	fin	11.363	1.01	13.0	1.03	

$sample_{10\mu l}$	band	% area	$r_{w/o\ topo}$	% $area_l$	$r_{l\ w/o\ topo}$	$r_{fin/ini}$
w/o $topo_{15}$	ini	2.816	1			2.98
w/o $topo_{15}$	fin	8.38	1	11.2	1	
0.1x $topo_{15}$	ini	2.80	0.99			3.41
0.1x $topo_{15}$	fin	9.55	1.14	12.4	1.10	
NEB_5	ini	2.88	1.02			3.82
NEB_5	fin	11.02	1.31	13.9	1.24	
NEB_{10}	ini	2.68	0.95			4.77
NEB_{10}	fin	12.81	1.53	15.5	1.38	
NEB_{15}	ini	2.45	0.87			5.98
NEB_{15}	fin	14.67	1.75	17.1	1.53	
NEB_{30}	ini	2.28	0.81			6.44
NEB_{30}	fin	14.71	1.75	16.0	1.52	
MB_{15}	ini	2.94	1.04			3.41
MB_{15}	fin	10.02	1.20	13.0	1.16	

Table B.1: Results for 2 μl and 10 μl lanes made from the intensity profiles. % area is to the area of the total area. $r_{w/o\ topo}$ is the relative value compared to the sample w/o topoisomerase calculated with the %area values. % $area_l$ is the sum for each lane (initial plus final band). $r_{l\ w/o\ topo}$ is again the relative value but per lane. $r_{fin/ini}$ is the initial band relative to the final band.

Bibliography

[1] B. Alberts, A. Johnson, J. Lewis, M. Raff, K. Roberts, and J. D. Watson. *Molecular biology of the cell*. Garland Science, Taylor & Francis Group, 5th edition, 2008.

[2] Charles L. Asbury, Adrian N. Fehr, and Steven M. Block. Kinesin moves by an asymmetric hand-over-hand mechanism. *Science*, 302:2130 – 2134, December 2003.

[3] A. Ashkin. Forces of a single-beam gradient laser trap on a dielectric sphere in the ray optics regime. *Biophys. J.*, 61:559 – 582, February 1992.

[4] A. Ashkin. Optical trapping and manipulation of neutral particles using lasers. *Proc. Natl. Acad. Sci. U S A*, 94:4853 – 4860, May 1997.

[5] A. Ashkin, J. M. Dziedzic, J. E. Bjorkholm, and S. Chu. Observation of a single-beam gradient force optical trap for dielectric particles. *Opt. Lett.*, 11:288 – 290, 1986.

[6] Lu Bai, Thomas J. Santangelo, and Michelle D. Wang. Single-molecule analysis of rna polymerase transcription. *Annu. Rev. Biophys. Biomol. Struct.*, 35:343 – 360, February 2006.

[7] Christoph Baumann, Roman Körner, Kay Hofmann, and Erich A. Nigg. Pich, a centromere-associated snf2 family atpase, is regulated by plk1 and required for the spindle checkpoint. *Cell*, 128:101 – 114, January 2007.

[8] J. F. Beausang, C. Zurla, L. Finzi, L. Sullivan, and P. C. Nelson. Elementary simulation of tethered brownian motion. *Am. J. Phys.*, 75(6):520 – 523, June 2007.

[9] S. Blumberg, A. Gajraj, M. W. Pennington, and J.-C. Meiners. Three-dimensional characterization of tethered microspheres by total internal reflection fluorescence microscopy. *Biophysical Journal*, 89:1272 – 1281, August 2005.

[10] James J. Champoux. Dna topoisomerases: Structure, function, and mechanism. *Annu. Rev. Biochem.*, 70:369 – 413, 2001.

[11] James J. Champoux. Type ia dna topoisomerases: Strictly one step at a time. *PNAS*, 99(19):11998 – 12000, September 2002.

[12] Kok-Lung Chan, Phillip S. North, and Ian D. Hickson. Blm is required for faithful chromosome segregation and its localization defines a class of ultrafine anaphase bridges. *EMBO*, 26:3397 – 3409, June 2007.

[13] Michael K. Cheezum, William F. Walker, and William H. Guilford. Quantitative comparison of algorithms for tracking single fluorescent particles. *Biophysical Journal*, 81:2378 – 2388, October 2001.

[14] Peter Chi, Youngho Kwon, Changhyun Seong, Anastasiya Epshtein, Isabel Lam, Patrick Sung, and Hannah L. Klein. Yeast recombination factor rdh54 functionally interacts with the rad51 recombinase and catalyzes rad51 removal from dna. *Jorunal of biological chemistry*, 281:26268 – 26279, September 2006.

[15] Matthew J Comstock, Taekjip Ha, and Yann R Chemla. Ultrahigh-resolution optical trap with single-fluorophore sensitivity. *Nature Methods*, 8:335 – 340, April 2011.

[16] N. H. Dekker, V. V. Rybenkov, M. Duguet, N. J. Crisona, N. R. Cozzarelli, D. Bensimon, and V. Croquette. The mechanism of type ia topoisomerases. *PNAS*, 99(19):12126 – 12131, September 2002.

[17] K Gresty and R Dryden. Cell cycle figure. http://learninglab.co.uk/, 2001.

[18] Peter Gross, Niels Laurens, Lene B. Oddershede, Ulrich Bockelmann, Erwin J. G. Peterman, and Gijs J. L. Wuite. Quantifying how dna stretches, melts and changes under tension. *Nature Physics*, 7:731 – 736, May 2011.

[19] Yuwen Ke, Jae-Wan Huh, Ross Warrington, Bing Li, Nan Wu Mei Leng, Junmei Zhang, Haydn L Ball, Bing Li, and Hongtao Yu. Pich and blm limit histone association with anaphase centromeric dna threads and promote their resolution. *EMBO*, 30:3309 – 3321, July 2011.

[20] Wang JC. Kirkegaard K. Escherichia coli dna topoisomerase i catalyzed linking of single-stranded rings of complementary base sequences. *Nucleic Acids Res.*, 5(10):3811 – 3820, October 1978.

[21] Daniel A. Koster, Vincent Croquette, Cees Dekker, Stewart Shuman, and Nynke H. Dekker. Friction and torque govern the relaxation of dna supercoils by eukaryotic topoisomerase ib. *Nature*, 434(7033):671 – 674, 2005.

[22] Daniel A. Koster, Aurélien Crut, Stewart Shuman, Mary-Ann Bjornsti, and Nynke H. Dekker. Cellular strategies for regulating dna supercoiling: A single-molecule perspective. *Cell*, 142(4):519 – 530, 2010.

[23] Block Lab. Figure of kinesin. http://www.stanford.edu/group/blocklab/kinesin/kinesin.html, 2009.

[24] D. Y. Lee and D. A. Clayton. Properties of a primer rna-dna hybrid at the mouse mitochondrial dna leading-strand origin of replication. *The Journal of Biological Chemistry*, 271:24262–24269, September 1996.

[25] J. F. Marko and E. D. Siggia. Statistical mechanics of supercoiled dna. *APS*, 52(3):2912 – 2938, September 1995.

[26] J. F. Marko and E. D. Siggia. Stretching dna. *Macromolecules*, 28:8759–8770, 1995.

[27] Graham Milne. http://grahammilne.com/tracker.htm, August 2007.

[28] Graham Milne. *Optical Sorting and Manipulation of Microscopic Particles*. PhD thesis, University of St Andrews, March 2007.

[29] Philip C. Nelson, Chiara Zurla, Doriano Brogioli, John F. Beausang, Laura Finzi, and David Dunlap. Tethered particle motion as a diagnostic of dna tether length. *The Journal of Physical Chemistry B*, 110(34):17260 – 17267, 2006.

[30] Peter E. Nielsen, Michael Egholm, Rolf H. Berg, and Ole Buchardt. Sequence-selective recognition of dna by strand displacement with a thymine-substituted polyamide. *Science*, 254(5037):1497 – 1500, December 1991.

[31] Amitabh V. Nimonkar, Ichiro Amitani, Ronald J. Baskin, and Stephen C. Kowalczykowski. Single molecule imaging of tid1/rdh54, a rad54 homolog that translocates on duplex dna and can disrupt joint molecules. *Journal of biological chemistry*, 282:30776 – 30784, October 2007.

[32] Kamilla Nørregaard. Single molecule studies reveal that dna supercoiling sharpens the λ-switch. Master's thesis, Niels Bohr Institute, 2011.

[33] Clare O'Connor. Chromosome segregation in mitosis: The role of centromeres. http://www.nature.com/scitable/topicpage/chromosome-segregation-in-mitosis-the-role-of-242, 2008.

[34] Lene B. Oddershede. *Handbook of Molecular Biophysics. Methods and applications.*, chapter 6, pages 197 – 214. WILEY-VCH VErlag GmbH & Co. KGaA, Weinheim, 2009.

[35] J. H. Park and Y. J. Lee. Robust visual servoing for motion control of the ball on a plate. *Mechatronics*, 13(7):723 – 738, September 2003.

[36] T.K. Prasad, R. B. Robertson, M. L. Visnapuu, P. Chi, P. Sung, and E. C. Greene. A dna-translocating snf2 molecular motor: Saccharomyces cerevisiae rdh54 displays processive translocation and extrudes dna loops. *J. Mol. Biol.*, 369:940–953, June 2007.

[37] G. Roosen. Optical levitation of spheres. *Can. J. Phys.*, 57:1260 – 1279, 1979.

[38] D. E. Segall, P. C. Nelson, and R. Philips. Volume-exclusion effects in tethered-particle experiments: Bead size matters. *PRL*, 96:088306–1–0883064, March 2006.

[39] T. R. Strick, J.-F. Allemand, D. Bensimon, and V. Croquette. Behavior of supercoiled dna. *Biophysical Journal*, 74:2016–2028, April 1998.

[40] Akio Sugino, Craig L. Peebles, Kenneth N. Kreuzer, and Nicholas R. Cozzarelli. Mechanism of action of nalidixic acid: Purification of escherichia coli nala gene product and its relationship to dna gyrase and a novel nicking-closing enzyme. *Proc. Natl. Acad. Sci. U S A*, 74(11):4767 – 4771, November 1977.

[41] Simon F. Tolic-Nørrelykke, Mette B. Rasmussen, Francesco S. Pavone, Kirstine Berg-Sørensen, and Lene B. Oddershede. Stepwise bending of dna by a single tata-box binding protein. *Biophysical Journal*, 90:3694–3703, May 2006.

[42] A. A. Travers and J. M. T. Thompson. An introduction to the mechanics of dna. *Phil. Trans. R. Soc. Lond. A*, 362:1265 – 1279, May 2004.

[43] Joost van Mameren, Mauro Modesti, Roland Kanaar, Claire Wyman, Erwin J. G. Peterman, and Gijs J. L. Wuite. Counting rad51 proteins disassembling from nucleoprotein filaments under tension. *Nature*, 457:745 – 748, February 2009.

[44] A. M. van Oijen. Single-molecule approaches to characterizing kinetics of biomolecular interactions. *Current Opinion in Biotechnology*, 22:1–6, 2010.

[45] Seychelle M. Vos, Elsa M. Tretter, Bryan H. Schmidt, and James M. Berger. All tangled up: how cells direct, manage and exploit topoisomerase function. *Nature Reviews Molecular Cell Biology*, 12:827 – 841, December 2011.

[46] J. C. Wang. Cellular roles of dna topoisomerases: A molecular perspective. *Nat. Rev. Mol. Cell Biol.*, 3:430 – 440, June 2002.

[47] M. D. Wang, H. Yin, R. Landick, J. Gelles, and S. M. Block. Stretching dna with optical tweezers. *Biophysical Journal*, 72:1335–1346, March 1997.

[48] J. D. Watson and F. H. C. Crick. Molecular structure of nucleic acids. a structure for deoxyribose nucleic acid. *Nature*, 171:737 – 738, April 1953.

[49] Wikipedia. Figure of mitotic spindle. http://en.wikipedia.org/wiki/Spindle_apparatus, 2011.

[50] Mitsuhiro Yanagida. Clearing the way for mitosis: is cohesin a target? *Nature Reviews Molecular Cell Biology*, 10:489 – 496, July 2009.

[51] Bo Zhang, Josiane Zerubia, and Jean-Christophe Olivo-Marin. Gaussian approximations of fluorescence microscope point-spread function models. *Applied Optics*, 46:1819–1829, April 2007.

[52] National Science Foundation Zina Deretsky. Figure of kinetochore. http://phys.org/news/2010-11-tighter-cell-division.html, 2010.